SLOVAK UNIVERSITY OF TECHNOLOGY IN BRATISLAVA
FACULTY OF MATERIALS SCIENCE AND TECHNOLOGY IN TRNAVA

Kateryna Smyrnova

Dissertation Thesis Abstract

Microstructure and Properties of Multilayer Coatings of the WN/MeN Type Depending on the Elemental Composition of the Second Layer

to obtain the Academic Title of „doktor“ („philosophiae doctor“, abbreviated as „PhD.“)

in the doctorate degree study programme: 104250 Advanced Materials and Materials Design

in the field of study: Mechanical Engineering

Form of Study: full-time

Place and date: Trnava, 2023

Dissertation Thesis has been prepared at: Institute of Materials of Faculty of Materials Science and Technology in Trnava

Submitter: **Kateryna Smyrnova**
Institute of Materials
Faculty of Materials Science and Technology in Trnava
Jána Bottu 25, 917 24 Trnava

Supervisor: **Prof. Ing. Ľubomír Čaplovič, PhD.**
Institute of Materials
Faculty of Materials Science and Technology in Trnava
Jána Bottu 25, 917 24 Trnava

Opponents: .....
.....
.....
.....

Dissertation Thesis Abstract was sent: .....
(Date of sending)

Dissertation Thesis Defence will be held on .....
at.....h (am/pm) at .....
.....
(exact address where the dissertation thesis defence will take place)

.....
Prof. Ing. Miloš Čambál, CSc.
Dean of Faculty of Materials Science and Technology in Trnava

TABLE OF CONTENTS

INTRODUCTION

Transition metal nitrides have become an essential part of manufacturing technologies. Due to the increased demands for drilling and cutting tools operating at extreme machining temperatures and rates, protective coatings are extensively utilized to prolong the useful tool life and eliminate the need for lubricants. Hence, they decrease the environmental hazards and increase the quality of fabricated tools, ultimately reducing maintenance costs. Transition metal nitrides are very popular for this application and are actively studied by many experts in the field of materials science [1–4].

Monolayer nitrides, such as TiN, ZrN, and CrN, have been used for tribological applications for decades. However, numerous studies have demonstrated that alternating deposition of binary nitride layers produces multilayer coatings with superior properties, i.e., TiN/ZrN, TiN/CrN, CrN/ZrN, MoN/CrN, and TiN/MoN [4–8]. That resulted in the widespread interest in multilayer architecture since it provides high hardness, wear resistance, and thermal stability. It can effectively hinder crack propagation due to the numerous interfaces between layers and grain boundaries [9]. On the other hand, the multilayer concept unites properties specific to each individual layer in a new structure with unique and enhanced characteristics [10,11].

Analysis of the literature has revealed that tungsten nitride is a promising potential material for protective coatings since it has high melting temperature, enhanced hardness, oxidation resistance, and thermal stability [12,13]. It was found that at 700 ˚C, the cubic W_2N did not show signs of decomposition and maintained a high hardness of about 22 GPa [14]. Such characteristics are suitable for industry-related applications. Moreover, considering the advantages of the multilayer approach, it can be assumed that using WN as one of the constituent layers must result in a material with superior ultimate properties. Also, it is worth mentioning that no reports on WN-based binary multilayers synthesized by cathodic-arc physical vapor deposition (CA-PVD) have been found.

The PhD thesis “Microstructure and properties of multilayer coatings of the WN/MeN type depending on the elemental composition of the second layer” deals with nanoscale WN/MeN (Me = Cr, Zr, Mo, Nb) multilayer coatings synthesized by CA-PVD technique. The effect of a second MeN layer in WN-based multilayers on microstructure evolution, phase composition, mechanical properties, and tribological performance has been comprehensively investigated. The first-principles calculations of random $W_{1-y}N_{1-x}$ ($0 \leq x,y \leq 1$) phases were performed to gain more insight into the properties of deposited multilayers. Mainly to find the most favorable structure that could develop in the WN layers in the deposited multilayers. Moreover, an in-depth study of the influence of the negative bias voltage on phase composition, texture, mechanical properties, and room-temperature tribological performance of the CA-PVD WN/NbN coatings was performed. The work was supported by the EU NextGenerationEU through the Recovery and Resilience Plan for Slovakia under the project No. 09I03-03-V01-00027 and the National Scholarship Programme of the Slovak Republic for the Support of Mobility of Students, PhD Students, University Teachers, Researchers and Artists.

This work consists of 5 chapters. The first chapter is devoted to a review of multilayer nitride coatings and binary nitrides, which were chosen as the second layer for different WN-based multilayer systems. The second chapter describes the main goals of the PhD thesis. The third chapter discusses the methodology used to investigate the structure and properties of the deposited coating. The fourth chapter reports all the results of a comprehensive study of the WN-based multilayer nanostructured coatings. Finally, conclusions with the purpose of future research are provided.

1. OVERVIEW OF THE TRANSITION METAL NITRIDES

Overall, nitrides are simple metal structures with smaller in size nitrogen atoms that are placed in the interstitial sites (octahedral holes) of a close-packed lattice. Metal nitrides typically have face-centered cubic (fcc) or hexagonal close-packed (hcp) metal lattices with non-metal atoms, which are

more or less randomly distributed in the interstitial gaps. Three combinations of chemical bonds between atoms are possible depending on the metal that reacts with nitrogen: metallic covalent and ionic. Generally, transition metal nitrides have a combination of different types of chemical bonds [1]. When we consider transition metals of the IV-VI groups in the direction Ti $\rightarrow$ Cr, Zr $\rightarrow$ Mo, and Hf $\rightarrow$ W, the statistical weight of the sp^3 and d^5 configurations gradually decreases and increases, respectively. This means that Me-Me interactions become more potent in MeN compounds while covalent and ionic bonds weaken. These materials are characterized by a high melting point, hardness, corrosion resistance, and good electrical and thermal conductivity [15,16]. Due to the universal and simultaneously unique properties, nitrides of transition metals are widely applied as structural materials in engineering, nuclear, and chemical industries, in the production of abrasives, cutting tools, wear-resistant materials, and so forth [17,18].

Transition metal nitrides in the form of multilayer coatings have been actively investigated since the last quarter of the 20th century due to the numerous possible applications [19,20]. It was found that multilayer nitrides demonstrate excellent durability, wear and corrosion resistance, mechanical, optical, electronic, and magnetic properties [21,22]. An abiding scientific interest in these types of coatings can be explained by the fact that such structures as a whole can demonstrate excellent physical-mechanical characteristics that are unusual for their individual constituents. Interfaces between layers in multilayers have sufficiently strong bonds, preventing the formation and propagation of dislocations and nanocracks. The properties of multilayer coatings can be tuned by varying the size of grains and their quantity, total coating thickness, bilayer period, composition of each layer, and the structure of interfaces. Therefore, it is essential to choose the optimal deposition parameters in order to synthesize coatings with the best performance.

Among the various compositions of the binary multilayer nitride coatings, WN-based ones have not been comprehensively studied, even though tungsten nitride exhibits high hardness, chemical stability, and tribological performance [23]. The observed diversity among the WN-based multilayer systems appears to be limited. However, all coatings exhibited high hardness, elastic strain to failure (H/E_r), resistance to plastic deformation (H^3/E_r^2), relatively low coefficient of friction (COF), and specific wear rate. The exhibited properties suggest the potential of WN-based multilayer coatings for tribological applications, yet further comprehensive studies of the structure-properties relationships are required.

2. OBJECTIVES OF THE PhD THESIS

Analysis of the previous studies has revealed that wear-resistant and hard WN plays a crucial role in the high performance of the binary nitride multilayers. However, the second layer is also undoubtedly significant. The effect of its composition on the ultimate properties of the coating is noteworthy and should be thoroughly investigated. Interestingly, all WN-based binary nitride multilayers addressed in previous works were synthesized solely by magnetron sputtering and ion-beam-assisted deposition methods. The cathodic-arc physical vapor deposition (CA-PVD) has never been used to produce such coating systems. Therefore, the following objectives of the PhD thesis entitled "Microstructure and Properties of Multilayer Coatings of the WN/MeN Type Depending on the Elemental Composition of the Second Layer" were defined:

- to synthesize WN/MeN (Me = Zr, Cr, Mo, Nb) multilayer coatings by cathodic-arc evaporation technique;
- to perform first-principles calculations of the cubic random $W_{1-y}N_{1-x}$, $0 \leq x,y \leq 1$, phases to study their stability and structural and mechanical properties;
- to study phase composition, structural features, mechanical and tribological properties of WN-based multilayers deposited at the same conditions;

- to analyze the microstructure of coatings using high-resolution transmission electron microscopy and scanning transmission electron microscopy;
- to determine the relationship between microstructure and tribomechanical properties of different multilayer systems;
- to fabricate the coating that demonstrated the best tribomechanical properties by CA-PVD at various negative bias voltages;
- to comprehensively study the phase composition, texture, microstructure, mechanical properties, and room-temperature wear behavior of the CA-PVD WN/NbN coatings;
- to investigate the texture evolution with coating thickness and determine the relationship between wear behavior and microstructural features.

3. EXPERIMENTAL METHODS AND MATERIALS

For this study, two deposition sets were conducted. For the first part of the research, the WN/MeN (Me = Zr, Cr, Mo, Zr) coatings were fabricated by a cathodic-arc0 evaporation method using an upgraded "Bulat-6" device using targets of pure metals. The X6CrNiTi18-11 stainless-steel was used a substrate. The angle between two cathodes was set at 90˚. The deposition parameters were the following: arc currents were set at 100 A, bias voltage was -150 V, working pressure was 0.73 Pa, the substrate temperature was kept at 400 ºC, the substrate-target distance was 60 mm, substrate rotation was 7 rpm, and the total deposition time was maintained at 60 min.

For the second part of the study, WN/NbN nanolayer coatings were deposited by CA-PVD technique using the same device. W (99.5%) and Nb (99.5%) were used as targets. The material of the substrate was X6CrNiTi18-11 stainless-steel. Three WN/NbN coatings were prepared in the nitrogen atmosphere by changing the negative substrate bias voltage, U_s. Multilayers deposited at –50 V, –100 V, and –200 V were designated M-50, M-100, and M-200, respectively. In order to synthesize a nanolayer architecture, the substrate holder was constantly rotated at the rate of 7 rpm. The working gas pressure was 0.4 Pa. The temperature of the substrate during the deposition was fixed at 400 ºC. The arc current applied to W and NbN targets was 120 A. The total time of the coating deposition was maintained at 60 min.

The phase analysis of deposited coatings was conducted by Bragg–Brentano X-ray diffraction (XRD) and Grazing-Incidence X-ray diffraction (GIXRD) using Panalytical Empyrean X-ray diffractometer with Cu-Kα radiation. Residual stresses were evaluated via $\sin^2\psi$ measurements using the same device with Co X-Ray tube. The morphology and cross-sections of WN-based multilayers were studied via the JEOL JSM 7600F high-resolution field emission scanning electron microscope (SEM). It was equipped with the Oxford Instruments Inca Wave spectrometer for wavelength-dispersive X-ray spectroscopy (WDS), used for the chemical composition characterization. Auger analysis was carried out in a JEOL JAMP 9510-F field emission Auger microprobe. The topography and surface roughness were determined by the Zeiss LSM 700 scanning laser confocal microscope (LSCM) following the ISO 25178 standard. Lamella for the transmission electron microscope (TEM) observations were prepared by focused ion beam using SEM. The crystallographic characterization and phase identification of multilayers were carried out via TEM using JEOL JEM-ARM200CF. Energy-dispersive X-ray spectroscopy (EDS) was performed to obtain elemental mapping images. Results were processed using Gatan DigitalMicrograph® and CrysTBox. First-principles calculations of the random cubic B1- $W_{1-y}N_{1-x}$, $0 \le x, y \le 1$, compounds were performed using the pseudopotential code "Quantum ESPRESSO". Nanohardness and elastic modulus were evaluated using the Anton Paar NHT^2 nanoindenter equipped with a Berkovich tip at the load of 10 mN. The load-displacement curves were processed by the Oliver and Pharr method. Scratch testing was conducted to determine the substrate/coating adhesion strength by Bruker UMT Tribolab device adjusted to scratch test

configuration with Rockwell-C type indenter. The detailed examination of the first cracks and delaminations with a determination of critical loads was conducted by SEM. The adhesion of the WN/NbN coating system to the substrate was additionally examined by the Daimler–Benz test (Škoda RB-1 hardness tester). Furthermore, the character of cracks around imprints was evaluated with SEM according to the VDI 3198 standard. The COF and wear resistance were studied via the ball-on-disk tests (Bruker UMT Tribolab Tribometer). The counter-body was an Al_2O_3 ball with a diameter of 5 mm (first part of the research) and 100Cr6 steal ball with a diameter of 6.3 mm (second part of the research). The wear rate, w_s, was calculated in accordance with the ASTM G99-17 standard. Wear volumes were measured by Zeiss LSM 700 LSCM. The Raman spectra have been measured with the WiTeC Alpha 300R microRaman system. The laser source with a wavelength of 532 nm and a power of 1 mW has been chosen.

4. RESULTS AND DISCUSSION

4.1. Effect of the Second Layer on Properties of WN/MeN (Me = Zr, Cr, Mo, Nb) Multilayers

4.1.1. Structural features

The cross-sectional morphologies of the WN/ZrN, WN/CrN, WN/MoN, and WN/NbN coatings are presented in Fig. 1. The WN/ZrN, WN/CrN, WN/MoN, and WN/NbN coatings demonstrated a well-defined layered structure with dense columnar growth. Multilayers had different bilayer period (Λ): 14.5 nm (WN/CrN), 15.3 nm (WN/MoN), 20 nm (WN/ZrN), and 21.1 nm (WN/NbN). Respectively, the total coating thicknesses ranged from 4.7 μm to 5.6 μm. The decrease in bilayer thickness of multilayers deposited from Cr and Mo cathodes may be explained by the difference in kinetic energies of ions generated during the cathodic arc evaporation. Its distinctive feature is the formation of ions with high energies varying from 20 to 200 eV [24].

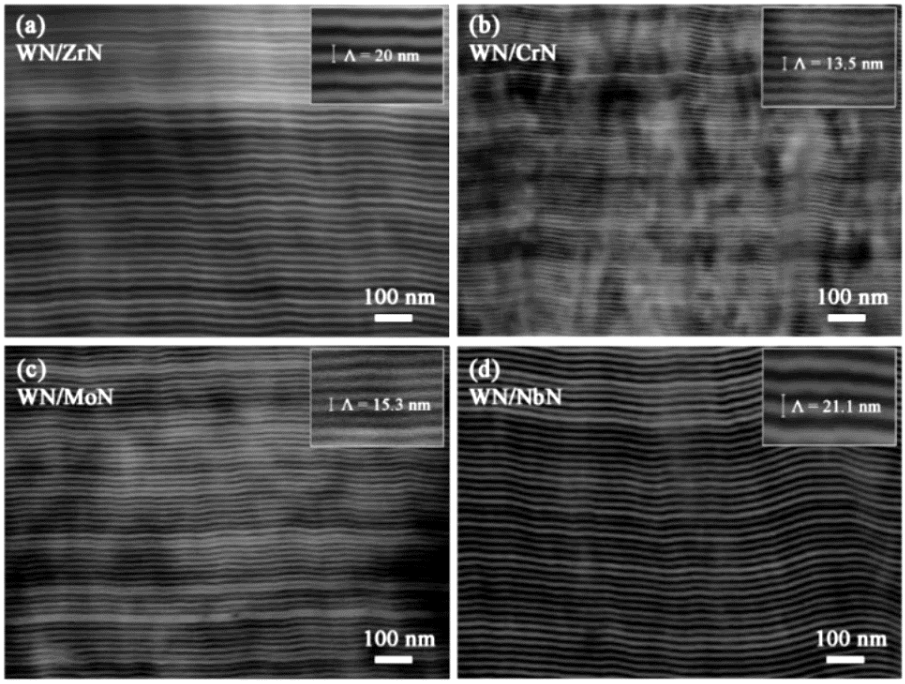

Fig. 1. *Cross-sectional SEM images of WN-based multilayer coating systems. Bilayer thicknesses are p2resented in the inserts.*

The surface roughness of WN/ZrN, WN/CrN, WN/MoN, and WN/NbN was measured to be about 67 nm, 46 nm, 43 nm, and 32 nm, respectively. Nanoscale WN-based multilayer systems with Zr and Nb were the coarsest and the smoothest, respectively. The chemical composition of the deposited multilayers was determined by the WDS method (Table 1). Coatings had almost the same contents of W and N, except for the WN/CrN one. It contained a high tungsten concentration (37.3 at.%). Such peculiarity could be caused by the resputtering process due to significant differences in the kinetic energies and sizes of W and Cr ions. According to the Auger in-depth element profiles, the nitrogen profile has reached its minimum in the layer containing tungsten, which indirectly confirms the formation of the cubic W_2N phase, in which N atoms occupy half of the octahedral sites.

Table 1. *Chemical composition of the WN/MeN (Me = Zr, Cr, Mo, Nb) multilayers.*

Coating	Element Concentration (at.%)					
	W	N	Cr	Mo	Nb	Zr
WN/CrN	37.3	51.4	11.3	-		-
WN/MoN	26.4	54.2	-	19.4	-	-
WN/NbN	27.2	52.4	-	-	20.4	-
WN/ZrN	26.4	52.4	-	-	-	21.2

The XRD spectra of the nanostructured WN/MeN (Me = Zr, Cr, Mo, and Nb) coatings are presented in Fig. 2. The phase analysis of the nanostructured WN/MeN (Me = Zr, Cr, Mo, and Nb) coatings demonstrated that the common for all multilayers WN layer had the fcc NaCl-type β-W_2N phase. However, the second distinguishing nitride layer was unique for each coating system. Regarding the structure of the second layer, coatings could be roughly classified into two groups. The general trend inherent in the first group of multilayers (WN/ZrN and WN/CrN) was an isostructural growth during deposition. The XRD results showed that CrN and ZrN layers, similarly to WN, developed the NaCl-fcc $Fm\bar{3}m$ structure. A distinctive feature of the multilayers included in the second group was a polycrystalline structure consisting of fcc and hexagonal phases in MoN and NbN layers. The WN/NbN coating developed

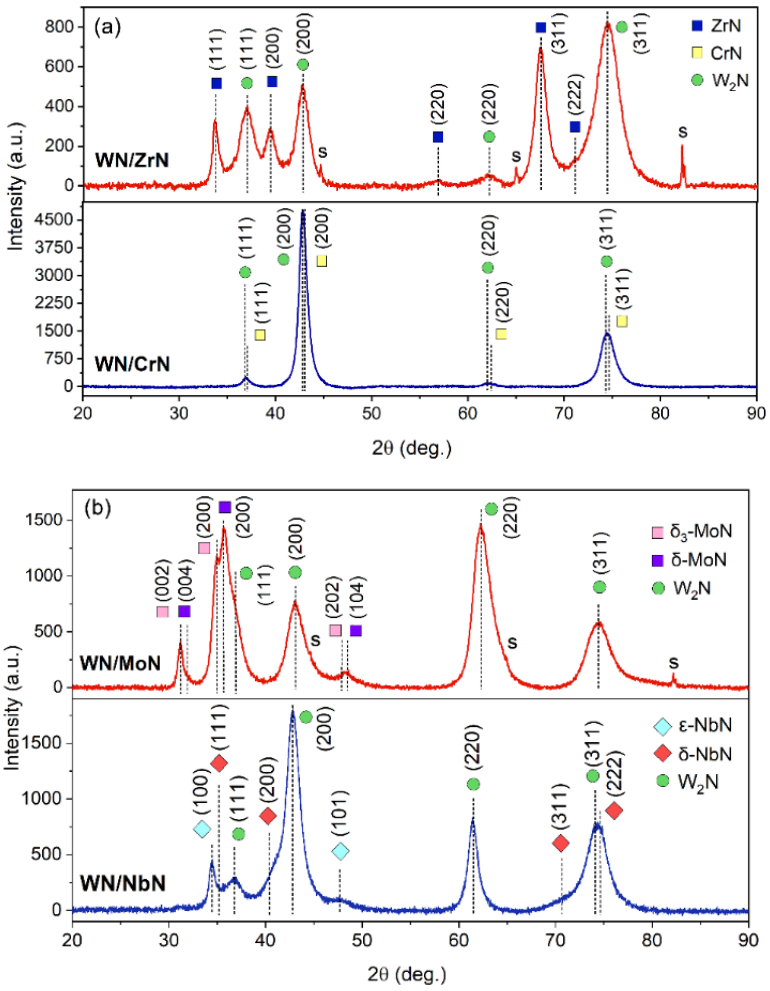

Fig. 2. *XRD patterns of the WN-based multilayer coatings: WN/CrN and WN/ZrN (a); WN/MoN and WN/NbN (b).*

the fcc β-W_2N, fcc δ-NbN (No. 225, $Fm\bar{3}m$), and hexagonal ε-NbN (No. 194, $P6_3/mmc$) phases. The WN/MoN coating consisted of the fcc-W_2N, and hexagonal δ-MoN (No. 162, $P\bar{3}1m$) and δ_3-MoN (No. 186, $P6_3mc$) phases. The WN/CrN and WN/ZrN coatings developed compressive residual stresses of about −7462.7 ± 245.5 MPa and −4865.6 ± 306.6 MPa. The WN/MoN coating had residual stress of about −7226.2 ± 618.8 MPa. Moreover, according to the $\sin^2\psi$ measurements, the NbN-containing coating exhibited compressive internal stresses of about −9235.6 ± 233.1 MPa.

The cross-sectional bright-field STEM images of WN/NbN and WN/MoN coatings demonstrated that the bilayer periods of those multilayers were 20.05 nm and 15.9 nm, respectively, which was in good agreement with SEM observations. The STEM-EDS results for the WN layer in both coatings showed that the W/N ratio was approximately 2, proving the formation of the W_2N phase.

Fig. 3 presents the cross-sectional HR-TEM and HAADF STEM images of the WN/NbN multilayer. From the point of crystallography, the estimation of fast Fourier transform (FFT)-HR-TEM of the WN layer (Fig. 3b) revealed the crystallite of the fcc W_2N phase, oriented along the [100] zone axis. In contrast, the NbN layers comprised both hexagonal ε-NbN and fcc δ-NbN phases. Due to the selected <110> orientation of TEM lamella, <110> NbN and <110> W_2N crystallites were predominant. Fig. 3d demonstrates the more detailed atomic resolution HAADF STEM image recorded from the fcc δ-NbN phase. The image shows columns of Nb atoms arranged in pseudo-hexagons, which is in agreement with <110>-oriented δ-NbN. The measured interplanar distances of d_{200} = 0.217 nm and d_{111} = 0.250 n were consistent with the XRD analysis. The typical microstructure of the CA-PVD WN/MoN multilayers studied by HR-TEM is presented in Fig. 3e-f. The WN layer consisted of β-W_2N phase. However, the MoN layer developed a complex structure, represented by three crystalline phases: fcc γ-Mo_2N and two hexagonal phases, δ-MoN and δ_3-MoN. The cubic molybdenum nitride was not detected in XRD patterns because of the small amount.

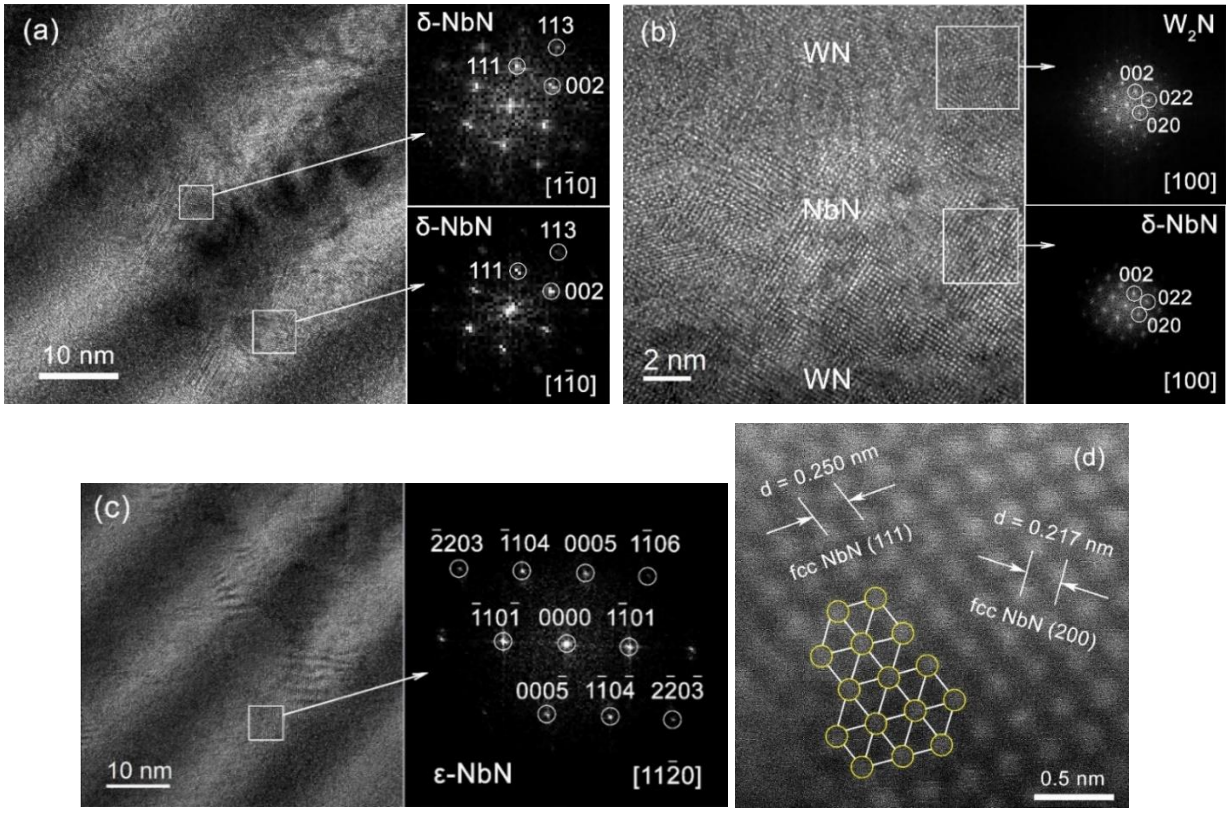

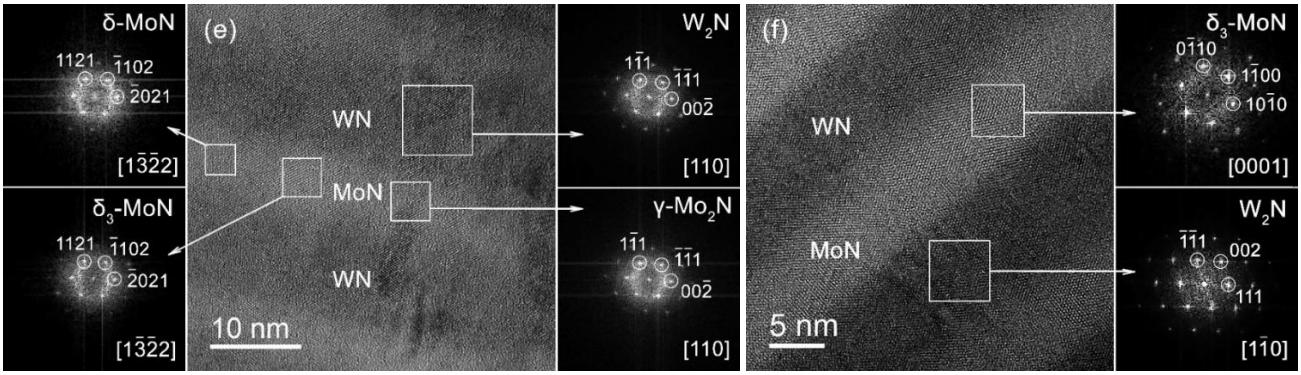

Fig. 3. *Cross-sectional HR-TEM images of the WN/NbN coating with relevant FFT patterns from different layers corresponding to [1$\bar{1}$0] zone axis of the cubic δ-NbN (a), [100] zone axis of W_2N and δ-NbN phases (b), and [110] zone axis of hexagonal ε-NbN (c). HAADF STEM image of the columns of Nb atoms in fcc δ-NbN lattice oriented along <110> direction (d). HR-TEM cross-sections of the WN/MoN multilayers with the corresponding FFT patterns featuring hexagonal δ-MoN and δ_3-MoN, and cubic γ-Mo_2N and W_2N phases (e); [0001] zone axis of δ_3-MoN phase and [1$\bar{1}$0] zone axis of the fcc W_2N (f).*

The stability and structural and mechanical properties of the cubic random $W_{1-y}N_{1-x}$, $0 \le x,y \le 1$, phases were studied by first-principles calculations. For WN_{1-x}, the lattice parameter decreases with increasing *x*, whereas the $H^f(x)$ has a minimum at $x = 0.5$ (Fig. 4). The stoichiometric phase cannot be synthesized because its formation energy is positive. For $WN_{0.5}$, the calculated lattice parameter was about 0.420 nm, which agreed well with experimentally evaluated results for studied multilayer systems. This indicated that WN layers in deposited coatings were composed of cubic WN_{1-x} structures with compositions close to $WN_{0.5}$.

The necessary and sufficient conditions for the elastic stability of a cubic crystal are $C_{11} - C_{12} > 0$, $C_{11} + 2C_{12} > 0$, $C_{44} > 0$. The values of C_{11}, C_{12}, and C_{44} were found to be 510.2, 236.1, and 122.6 GPa, respectively, and they clearly indicate that $WN_{0.5}$ is elastically stable. Using the calculated moduli B = 327.1 GPa, G = 129.1 GPa, and E = 342.3 GPa, the Pugh's ratio k = G/B of $WN_{0.5}$ was found to be about 0.39 and the Poisson's ratio σ = 0.33. These results suggest that $WN_{0.5}$ should be ductile material since $k < 0.6$ and $\sigma > 0.25$.

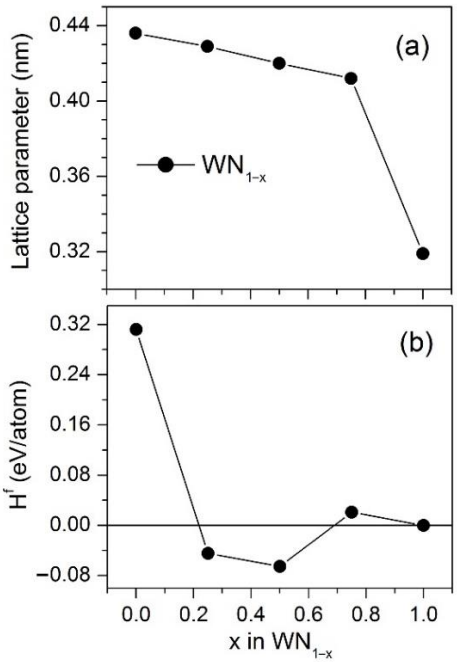

Fig. 4. *Lattice parameter (a) and energy of formation, H_f, (b) of random structures based on the $W_{16}N_{16}$ supercells.*

4.1.2. Mechanical properties

The nanohardness (H), elastic modulus (E), and H/E_r ratio (elastic strain to failure) are shown in Fig. 5. The hardness of the fcc-W_2N was reported to be around 24 GPa [23]. Therefore, all WN/MeN (Me = Zr, Cr, Mo, Nb) coating systems demonstrated enhanced hardness ranging from 33.3 ± 1.7 GPa to 37.3 ± 2.4 GPa. Such behavior can be explained by the mixed character of bonds in the constituent layers. The transition metal nitrides with the optimal proportion between covalent and metallic components are expected to have enhanced tribomechanical properties. Moreover, the hardness of the WN-based multilayer coatings superior to the reported respective single-layer coatings can also be related to the multilayer architecture. Nanoscale layers demonstrate an increase in the grain

boundaries' volume fraction, which refers to the Hall–Petch strengthening. Besides, alternating layers with different properties provide numerous interfaces between layers, hindering dislocation motions and crack propagations. Hardening arises due to coherency strains in the presence of crystalline interlayers and due to shear modulus differences between the different phases, i.e., Koehler hardening.

Coatings with a high H/E_r ratio are expected to have superior wear resistance. These conditions were met in the case of the WN/NbN multilayer (H/E_r = 0.093) (Fig. 5b). Thus, among the four WN-based multilayers, this coating system is expected to have enhanced resistance to wear. The described findings may be explained by the effect of the nanocomposite nature of the NbN layers consisting of two nanocrystalline phases (hexagonal and cubic).

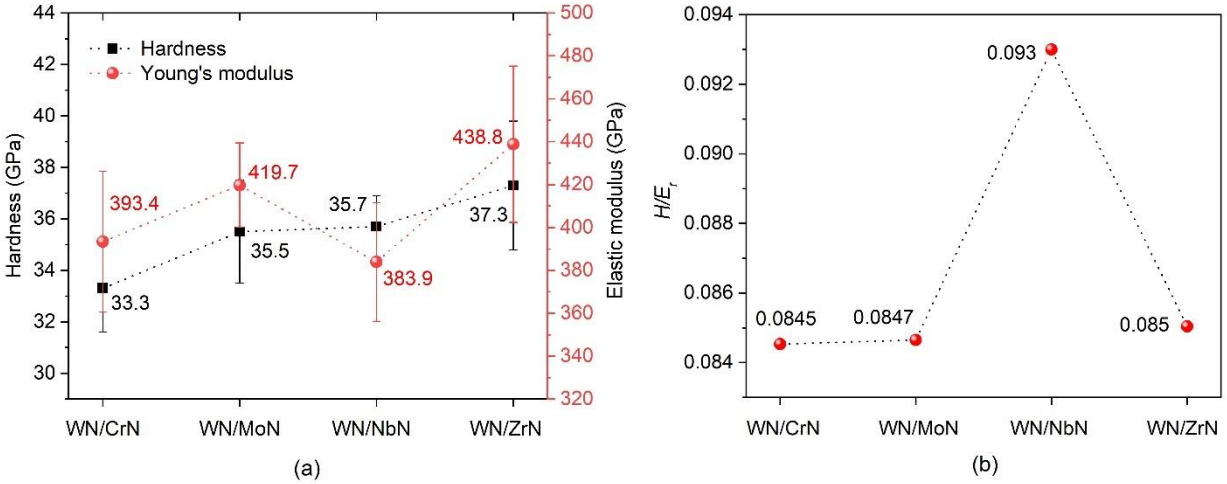

Fig. 5. *Hardness and elastic modulus (a) and H/E_r ratio (b) of the WN/MeN (Me = Zr, Cr, Mo, Nb) multilayer coatings*

4.1.3. Coating-substrate adhesion

The scratch test was employed to study coating-substrate adhesion. The surface roughness, mechanical strength, and substrate material directly influence the critical load values. According to the scratch test results, the total failure of the WN/ZrN, WN/CrN, WN/MoN, and WN/NbN coatings was recorded at the following L_3 values: 11.4 N, 15.0 N, 15.1 N, and 24.2 N, respectively. Hence, the WN/NbN multilayer demonstrated the best adhesion to the substrate, which was expected based on high mechanical properties and low surface roughness. Similarly, the WN/ZrN coating with the highest roughness and brittle nature showed the worst results. Moreover, the coating failure could be caused by the difference in elastic modulus values of the stainless-steel substrate and coating. The coating with NbN was not aggregated along the scratch groove and resisted the increasing load even after its exfoliation. It showed the narrowest scar and the shortest peripheral cracks. The Daimler–Benz test was additionally conducted to study the WN/NbN multilayer that demonstrated the best adhesion to the substrate during scratch testing. The results revealed no evidence of radial cracks and delamination near the indentation, classifying the coating adhesion as HF 1 that refers to the best adhesion. Therefore, the soft steel substrate vastly influenced the adhesion strength during the scratch test.

4.1.4. Friction performance

The wear behavior of the protective hard coatings can be assessed by two main parameters: friction coefficient and specific wear rate. Fig. 6 shows COF curves of the WN/MeN (Me = Zr, Cr, Mo, Nb) coatings. They were measured during the sliding of the Al_2O_3 ball against their surfaces. Among four WN-based multilayer systems, WN/ZrN had the worst friction performance (Table 2).

The explanation for this behavior may be the brittle nature of ZrN due to the prevalence of directional (covalent) bonding. Furthermore, it had the highest roughness. Even though WN/MoN multilayer had similar to WN/CrN mechanical properties and surface roughness, it exhibited the lowest COF. The reason for that was the formation of lubricant oxygen-deficient Magnéli-phases [8]. However, the friction coefficient of WN/MoN coating after 780 s began to rise to 0.66. That could mean delamination and gradual degradation. The COF curve of the WN/NbN system demonstrated a stable steady-state period till the end of the sliding. After running-in state, the fluctuations were due to the repeated formation and removal of Nb_2O_5 and WO_3 tribofilms, effectively resisting the shear load. Thus, the formation of the lubricious oxides contributed to high wear resistance.

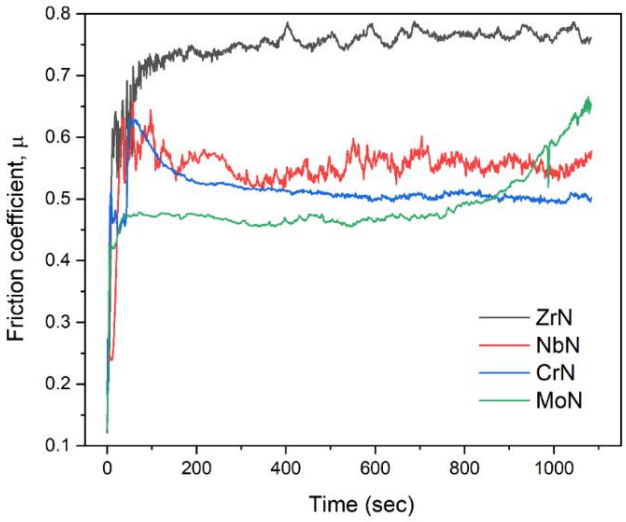

Fig. 6. *The friction coefficient curves of the WN/ZrN, WN/CrN, WN/MoN, and WN/NbN coatings on the stainless-steel substrate.*

4.1.5. Wear resistance

The typical wear tracks of WN/MeN (Me = Zr, Cr, Mo, Nb) coatings after the ball-on-disk test are shown in Fig. 7. Table 2 summarizes the values of average COF and specific wear rates.

Table 2. *Summary of the wear performance of the WN/MeN (Me = Cr, Zr, Mo, Nb) coatings.*

Parameter	**Coating system**			
	WN/ZrN	**WN/CrN**	**WN/MoN**	**WN/NbN**
Average friction coefficient	0.76	0.52	0.47	0.55
Specific wear rate of the coating, w_s (mm^3/Nm)	$3.8 \cdot 10^{-4}$	$1.1 \cdot 10^{-5}$	$8.6 \cdot 10^{-6}$	$1.7 \cdot 10^{-6}$

The WN/MoN coating had a higher wear rate of $8.6 \cdot 10^{-6}$ mm^3/Nm. Fig. 7 displays the smooth wear scar with wear debris and material pile-up around the track edges. Some tungsten content can still be seen, but mainly in the form of oxides. It can be concluded that the lubricant Mo_nO_{3n-1} phases participated in the coating protection from abrasive destruction. The observed plastic deformation of the contact area was attributed to the flow wear mode.

The CrN-containing multilayer system after the ball-on-disk test lost its integrity. There was still W detected, but the abrasive wear of the surface was clearly seen. The wear debris transferred from the mating alumina ball were attached to the surface. That describes the wear mode as mild abrasive/adhesive wear. The WN/CrN coating exhibited the second-lowest w_s value.

The WN/ZrN multilayer exhibited rough flake-like surface after Al_2O_3 ball sliding. This coating was worn the most. Due to numerous growth defects and the brittle character of hard ZrN-containing multilayer, severe abrasive wear was the principal wear mode. The flaky hard wear particles had a plowing effect on the coating surface, leading to severe damage.

SEM image of the WN/NbN wear track showed that the coating remained intact. The calculated w_s was the lowest among all coating systems ($1.7 \cdot 10^{-6}$ mm^3/Nm). Hence, the WN exhibited the best characteristics when combined with NbN in a nanoscale multilayer architecture. No signs of Fe, the

main element of the substrate, were detected on EDS maps. The presence of oxygen contamination could be related to the formation of lubricious Nb_2O_5 and WO_3 tribofilms appearing as islands, protecting the coating surface against destruction. Moreover, low roughness, high hardness and H/E_r ratio, ductile nature of NbN, and mixing of hard nanocrystalline ε-NbN and δ-NbN phases endowed this multilayer with superior wear resistance. Thus, the WN/NbN is expected to be a perfect candidate for anti-wear prospective coatings for tribological applications with extreme operating conditions.

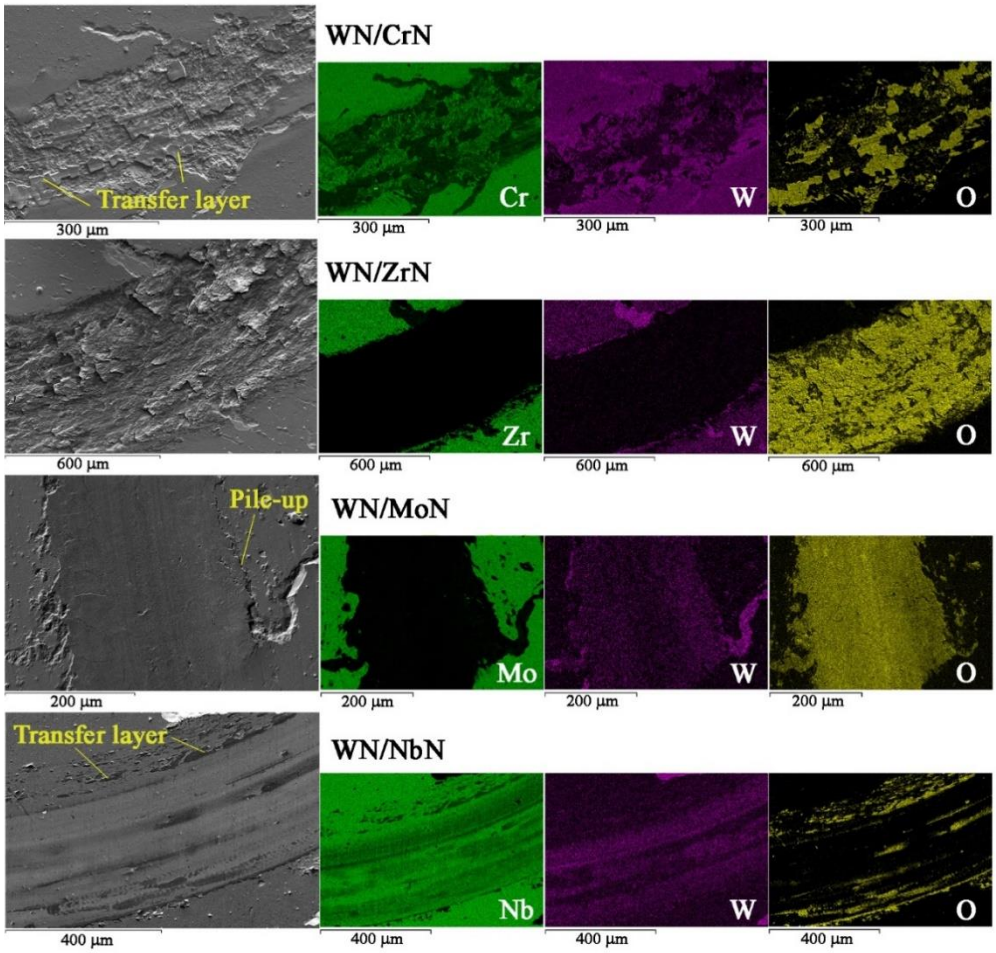

Fig. 7. *SEM images of wear scars (large images on the left) with EDS elemental maps (smaller images on the right) of the WN/MeN (Me = Zr, Cr, Mo, Nb) multilayer coatings.*

4.2. Effect of the Negative Bias Voltage on WN/NbN Coatings

4.2.1. Cross-sectional and surface morphology

WN/NbN coatings deposited at a bias voltage of –50, –100, and –200 V were designated M-50, M-100, and M-200, respectively. Fig. 8 represents cross-sectional SEM images at higher and lower magnifications. All coatings demonstrated a dense, well-defined layered structure without pores and cracks. Bright layers represented WN, and dark layers were assigned to NbN since the backscattered electron emission rate is higher for elements with higher atomic numbers. The bilayer period (Λ) varied depending on the applied substrate bias. Coating deposited at the highest U_s had the thinnest layers (Λ = 10 nm). However, the difference in the bilayer period of M-50 and M-100 samples was not drastic. Thus, deposited coatings had a nanolayered structure with Λ in the 10-15 nm range. Consequently, variations in the total coating thicknesses were observed, following the same trend as Λ: 4.7, 5.0, and 3.5 μm for M-50, M-100, and M-200, respectively. Applying higher negative bias voltage increases the resputtering rate of adatoms and densification caused by the bombardment ion flux effect. Table 3 provides the results of the chemical composition analysis determined by the WDS

method. The N concentration ranged from 49.1 to 51.1 at.%, indicating the nitrogen stoichiometry in the deposited multilayers. Applying the highest U_s of –200 V led to an increase in the W content up to 24 at.% with an associated decrease in the Nb and N concentrations. Such a high bias voltage improves energy transmission to the substrate.

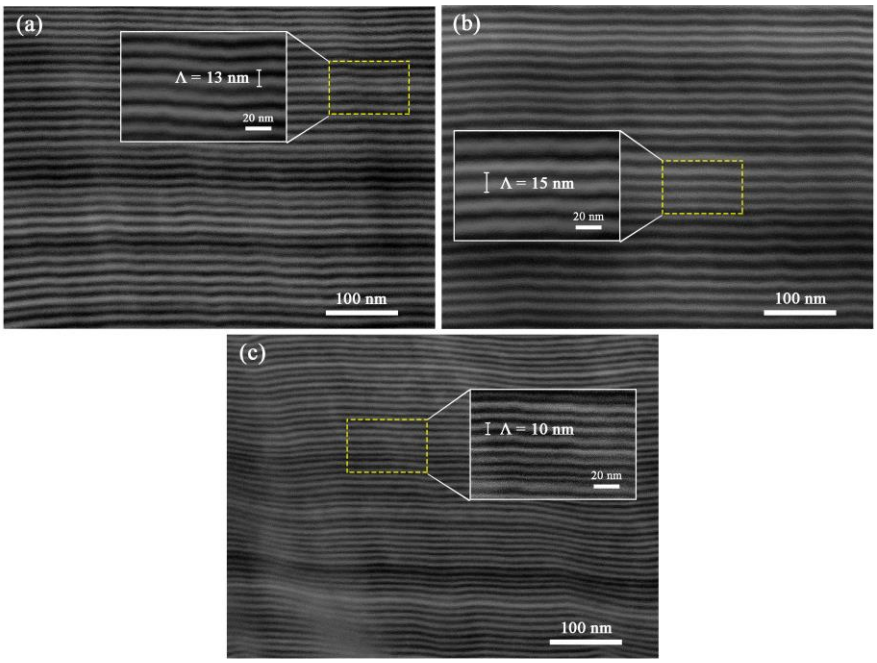

Fig. 8. *SEM cross-sectional micrographs of WN/NbN coatings deposited at different bias voltages: (a) –50 V, (b) –100 V, and (c) –200 V.*

Table 3. *Elemental composition of the WN/NbN coatings deposited at different negative substrate bias voltages.*

Coating	Element Concentration (at.%)		
	W	Nb	N
M-50	21.1	29.0	49.9
M-100	19.7	29.2	51.1
M-200	24.0	26.9	49.1

The analysis of the surface morphology of the WN/NbN coatings revealed that the average surface roughness (S_a) decreased with a rise in the negative substrate bias. A minimum value of about 36 nm was found for the M-200 coating. However, it is worth mentioning that although the sample prepared at the lowest bias voltage had a relatively rougher surface, the difference in S_a was negligible (41 and 36 nm). Such roughness values were obtained because the scan area was quite large (90 μm × 90 μm), and the macroparticles generated on the surface during the deposition process affected the results of the LSCM analysis. The reason for such a trend can be the densification of a structure due to the increase in the number of secondary nuclei, the higher energy of ions reaching the surface of the substrate, the higher flux of ionized species of the cathode material, and the resputtering of the growing coating occurring during the cathodic-arc deposition at a high negative bias voltage.

4.2.2. Microstructural characterization

The GIXRD patterns of the M-50, M-100, and M-200 coatings obtained at different ω angles of the incident beam are depicted in Fig. 9. All deposited nanolayers consisted of three phases: fcc β-W_2N (No. 225, $Fm\bar{3}m$, JCPDF 25–1257), fcc δ-NbN (No. 225, $Fm\bar{3}m$, JCPDS 38-1155), and

hexagonal ε-NbN (No. 194, $P6_3/mmc$, JCPDS 89-4757). The lattice parameters of all phases tended to gradually decrease with increasing the substrate bias voltage (Table 4). That could be associated with the formation of vacancies, intermixing between W- and Nb-based nitride layers, and the presence of compressive residual stresses. All coatings consisted of nanograins of similar sizes ranging from 2.8 to 4.3 nm. Measuring diffraction patterns at various incident ω angles allowed us to study in more detail the phase composition of deposited multilayers. Records obtained at ω = 0.5, 1, 4, 8, and 10 deg. could be associated with microstructural features at approximately the following penetration depths: 0.127, 0.254, 1.016, 2.027, and 2.530 μm.

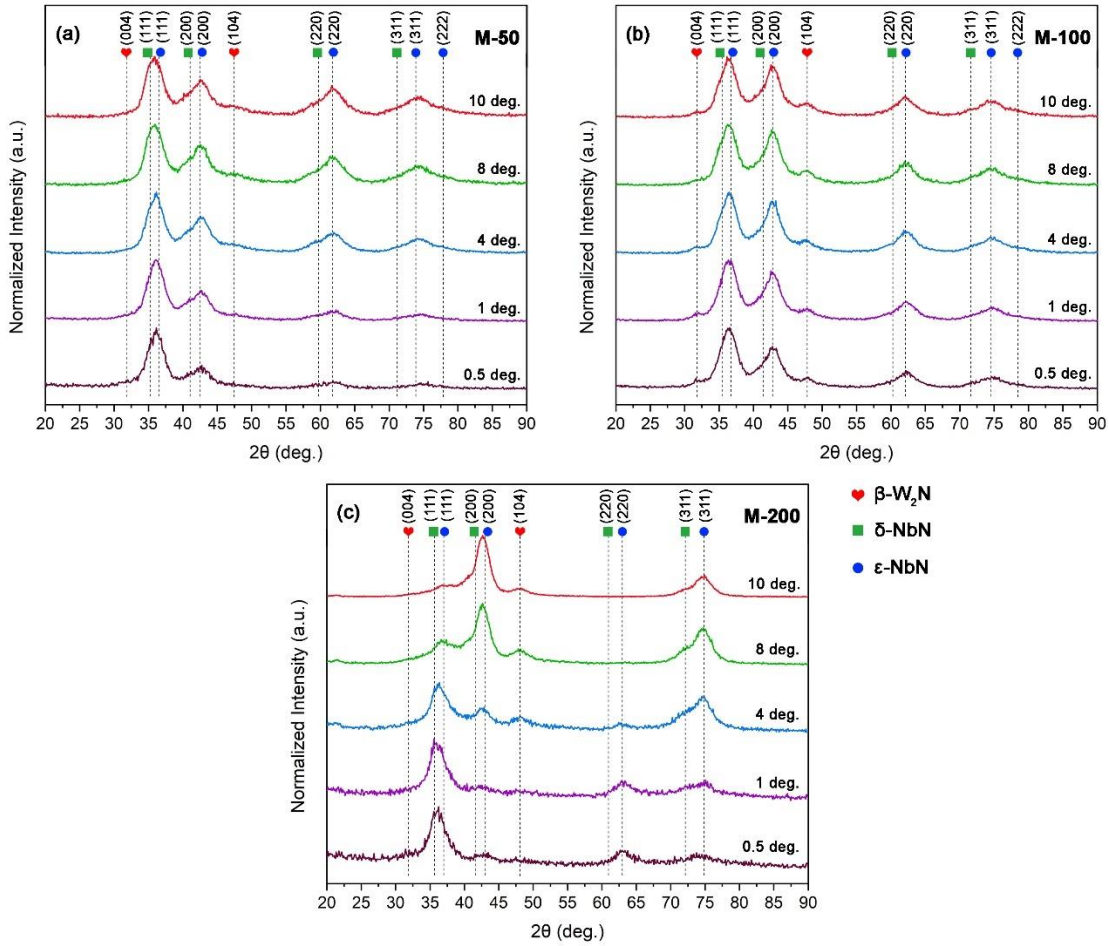

Fig. 9. *GIXRD patterns collected at ω angle from 0.5 to 10 deg. of the nanolayered WN/NbN coatings deposited at various bias voltages: (a) –50 V, (b) –100 V, and (c) –200 V.*

Table 4. *Summary of lattice parameters, grain sizes, and residual stresses of WN/NbN coatings deposited at different negative bias voltages.*

Coating	Lattice parameter (Å)			Grain size (nm)			Residual stresses (GPa)
	β-W_2N	ε-NbN	δ-NbN	β-W_2N	ε-NbN	δ-NbN	
M-50	4.238	2.988	11.274	4.386	3.2	2.8	–6.93 ± 0.88
M-100	4.219	2.969	11.252	4.358	3.4	4.3	–4.65 ± 0.29
M-200	4.194	2.938	11.229	4.332	3.7	3.6	–2.78 ± 0.56

Analysis of the GIXRD patterns of WN/NbN multilayers revealed that applying U_s of –100 V did not change the microstructure from the top layers to half the thickness of the coating (total thickness ≈ 5 μm). The intensity of the reflections from the hexagonal NbN phase in the M-100 coating

remained unchanged regardless of the ω angle. Furthermore, the coating demonstrated a (111) + (200) preferred orientation over the studied thicknesses with only a slight decrease in the (200) intensity.

GIXRD spectra of the M-50 multilayer obtained at the ω ranging from 4 – 10 deg. were characterized by the competitive growth of (111) and (200) planes. However, from a depth of about 250 nm, the intensity of (200), (220), and (311) peaks of the fcc phases and reflections from ε-NbN significantly decreased. Moreover, at a thickness of about 130 nm, grains developed a (111) preferred orientation. Such changes suggest a potential reduction in the density of defects and enhancement of the crystalline properties of a multilayer.

The M-200 multilayer showed an abrupt evolution of the crystallographic orientation throughout the coating thickness. The coating had a (200) preferred orientation at the initial growth stage. At a depth of about 2 μm from the surface, the intensity of (111) and (311) planes increased. An GIXRD pattern obtained at 1 μm from the surface (ω = 4 deg.) revealed that the (200) peaks continued to fade to the point that most grains were oriented within (111) and (311) directions. Finally, the structure of the area close to the surface (127 – 254 nm) was characterized by a strong (111) preferred orientation. Moreover, the ε-NbN reflections were almost undetectable. Similar behavior of the hexagonal NbN phase at the same ω angles was observed in the M-50 multilayer. That could mean that during deposition, at some critical thickness, the M-50 and M-200 coatings began to grow pseudoepitaxially at approximately the top 200 nm-thick layer.

It should be noted that the tendency for (111)-oriented grains to overgrow the (200)-oriented ones was inherent to all coatings to varying degrees. The alterations in the texture of the WN/NbN coatings throughout the thickness can be explained by anisotropies in atomistic processes taking place on different surfaces. The texture evolution in the M-200 coating was controlled solely by kinetic effects. However, at lower energies of bombarding ions, the balance between kinetic factors and thermodynamically driven growth governed the formation of the (111) + (200)-oriented grains. When (111) surfaces overgrew (200) planes, the kinetic effects came to the forefront. Moreover, the minimization of compressive residual stresses could govern the growth of (111) surfaces responsible for strain minimization. The residual stresses in deposited multilayers decreased from -6.93 ± 0.88 to -2.78 ± 0.56 GPa as the absolute value of the bias voltage increased. The texture features and increased mobility and diffusivity of adatoms contributed to the release of residual stresses.

The bright field TEM image of the M-200 cross-section was reported in Fig. 10. The WN layers had a slightly lower thickness compared to NbN ones. The average bilayer period was calculated to be approximately 10 nm, which agreed well with the SEM findings. The Fast Fourier Transformation (FFT) patterns from various areas of the sample were obtained to determine the phase composition of each individual nitride layer. WN layers represented by dark lines consisted of only NaCl-type β-W_2N crystallites. In contrast, the light layers ascribed to niobium nitride exhibited a more complex structure with nanocrystallites of the fcc δ-NbN and hexagonal ε-NbN phases. Similar to β-W_2N, cubic δ-NbN was oriented within the $[0\bar{1}1]$ direction of the <110> type. The distinct feature of the nanolayer coating deposited at the highest bias voltage was blurred interfaces between layers. This could be caused by intermixing due to high-energetic conditions during deposition. Moreover, STEM images revealed that despite a complex structure, a multilayer attempted to achieve semi-coherence in the crystallites.

4.2.3. Mechanical properties and adhesion

The mechanical properties of the nanolayer nitride coatings were assessed using four main parameters: nanohardness (H), elastic modulus (E_r), H/E_r, and H^3/E_r^2 ratios (Fig. 11). The nanohardness was the highest in the case of WN/NbN coating deposited at the highest bias voltage (36.6 ± 3.5 GPa), and the lowest for the M-100 multilayer (33.6 ± 3.0 GPa). However, high values of

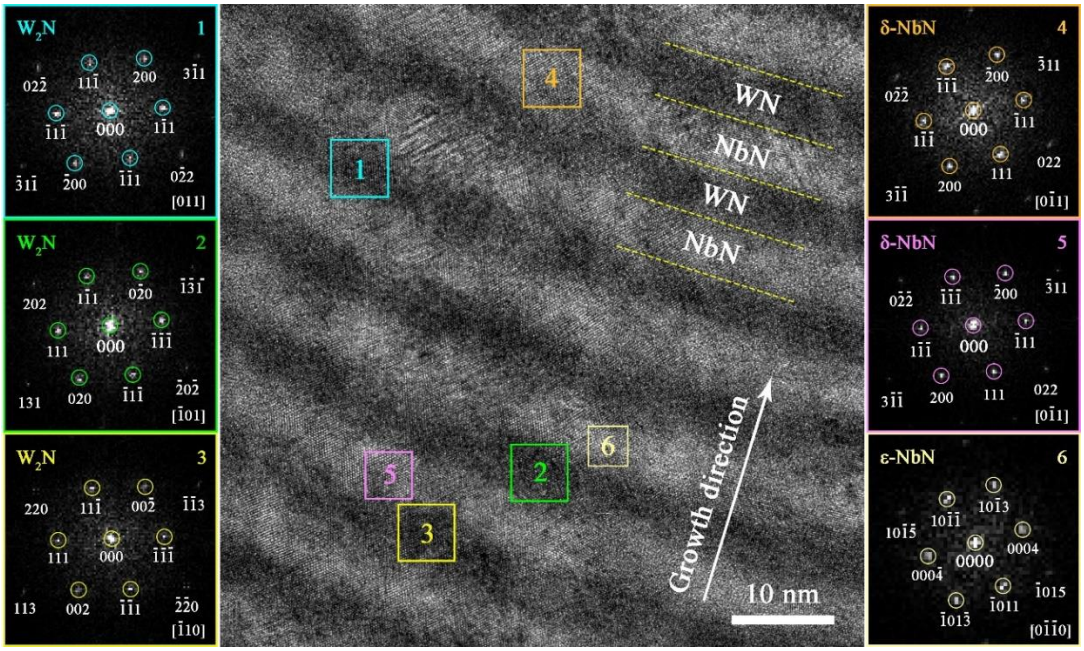

Fig. 10. *Cross-sectional bright field TEM image with FFT patterns from selected regions of the WN/NbN coating deposited at U_s = –200 V.*

H/E_r and H^3/E_r^2 ratios were found to be more essential for wear-resistant coatings. Among all WN/NbN multilayers, the M-50 sample demonstrated the maximum values of these parameters of about 0.085 and 0.254. Thus, it is expected to exhibit the best resistance to wear. Due to the multilayer architecture, costings have many interfaces that hinder the crack propagation and dislocation movement. They have a significant area of interphase boundaries and many defects at interfaces. Moreover, an increase in Λ from 10 and 15 nm led to a gradual decrease in hardness from 36.6 ± 3.5 to 33.6 ± 3.0 GPa. Another source of the hardness enhancement is the lattice misfit between adjacent phases [25] A fine-grained structure was also responsible for the high mechanical properties of the nanostructured WN/NbN coatings. Thus, high nanohardness, elastic strain to failure, and resistance to plastic deformation were attributed to the synergy of small grain sizes of all phases, low bilayer period, and a negligible amount of hard but brittle ε-NbN phase. It also should be noted that coatings with high mechanical properties (M-50 and M-200) had a (111) texture in the near-surface area.

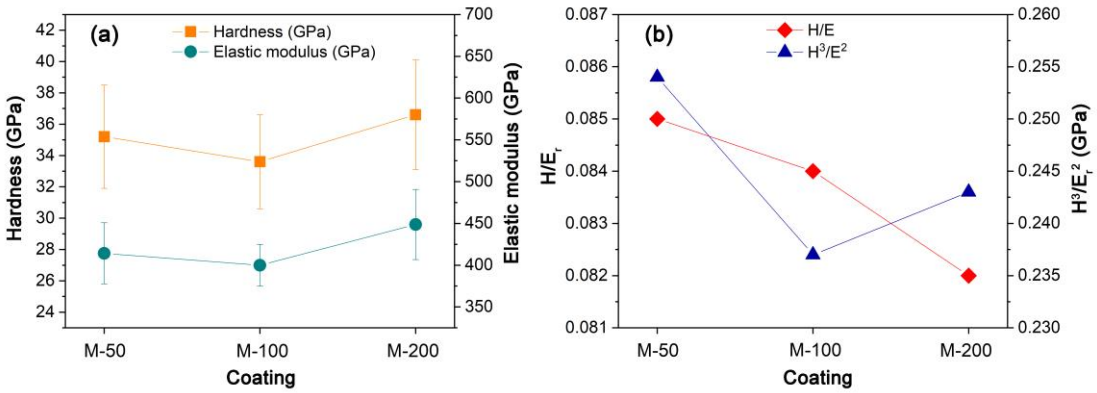

Fig. 11. *Mechanical properties of the WN/NbN multilayer coatings deposited at different negative bias voltages: hardness and elastic modulus (a), H/E_r and H^3/E_r^2 ratios (b).*

The adhesion strength of coating deposited at the lowest bias voltage has been classified as HF2, which is suitable for the protective coatings. Applying higher U_s deteriorated the coating/substrate adhesion. Coatings with the highest H/E_r ratio are expected to have the best elastic strain to failure, describing the amount of reversible deformation a material can undergo under stress without permanent damage. According to the results of nanoindentation tests, the adhesion results agreed well with the H/E_r ratio values since the coating obtained at the M-50 coating exhibited the most robust adhesion.

4.2.4. Tribological properties

The friction behavior of the steady-state phase varied for different coatings. The COF curve of the M-50 coating first had a slight ascending trend with some spikes during the steady-state part up to 300 s of sliding. After the contact between multilayer and steel counterbody surfaces was optimized, the COF decreased to approximately 0.7 and was stable until the end of the test. The M-100 multilayer demonstrated irregular and unstable friction behavior. The COF constantly rose from 0.5 to 0.75. The curve exhibited some discontinuance character with sharp fluctuations. That could be caused by local failure of the layer at some places and even coating delamination since the friction performance continued to worsen after those break-down events. Finally, the steady state of the COF curve of the M-200 coating first had an ascending character. However, it stabilized for the rest of the sliding with some local fluctuations, which could be related to the alternate failure of different individual layers and continuous formation and removal of WO_3 and N_2O_5, tribo-oxides. Thus, among all multilayers, the coating deposited at $U_s = -50$ V demonstrated the most stable friction performance, with the lowest COF at longer distances until the end of the sliding against a steel ball.

The wear behavior of the CA-PVD WN/NbN coatings was assessed by ball-on-disk tests using a stainless-steel counterbody. The SEM images of the worn surfaces and EDS elemental maps (W, Nb, Fe, O) of multilayers deposited at different substrate bias voltages are shown in Fig. 12. Analysis of wear scars of three WN/NbN coatings revealed different wear mechanisms and wear resistance.

The coating deposited at $U_s = -50$ V exhibited the least damaged surface after sliding a steel ball. The wear track was smooth without signs of coating delamination. The scar profile was shallow (Fig.13a). These parameters resulted in the lowest specific wear rate of $1.9 \cdot 10^{-6}$ mm^3/Nm. Fig. 12a showed only fine particles in small amounts. Those debris were oxides of tungsten and niobium, and no iron was detected on the wear scar area. These features indicate that the primary wear mechanism of the M-50 coating was oxidative wear (Fig. 13b). At low speeds below 1 m/s, the temperatures are not high enough to cause a direct oxidation of the highest surface irregularities. The process occurs due to the oxidation of the accumulated wear debris. When oxide films grown on asperities reach a critical thickness of around a few nanometers, they detach from the worn surface in the form of flaky oxide wear particles, which subsequently compact and create oxide “islands”. Observed oxide wear particles could be WO_3 and N_2O_5, known for their lubricious properties. These oxides can wear out fast, but also take a few microseconds to regrow. Moreover, the M-50 sample was characterized by the highest elastic strain to failure and resistance to plastic deformation, which also contributed to its superior wear resistance. This coating also had the high compressive residual stress, which is favorable for tribological applications, since it may enhance mechanical properties and crack resistance [26].

SEM images of the wear track provided Fig. 12b and the scar profiles presented in Fig. 13a of the M-100 revealed that it had the worst wear resistance. The depth and width of the wear scar had the greatest values, which attributed to the highest specific wear rate of this coating was $4.1 \cdot 10^{-6}$ mm^3/Nm. However, it is still within the moderate wear range. As noted above, the resistance to plastic deformation, represented by the H^3/E_r^2 ratio, was the lowest for this multilayer (Fig. 11b), which was found to be an indicator of low wear resistance. The highest amount of the brittle and hard hexagonal NbN phase with an average grain size of about 4 nm in this multilayer contributed to the widest groove and coating delamination. Hard and small grains acted as hard inclusions. Thus, the dominant wear

mechanism was fatigue wear, but the oxidative mode was also present, reducing the severity of wear (Fig. 13c).

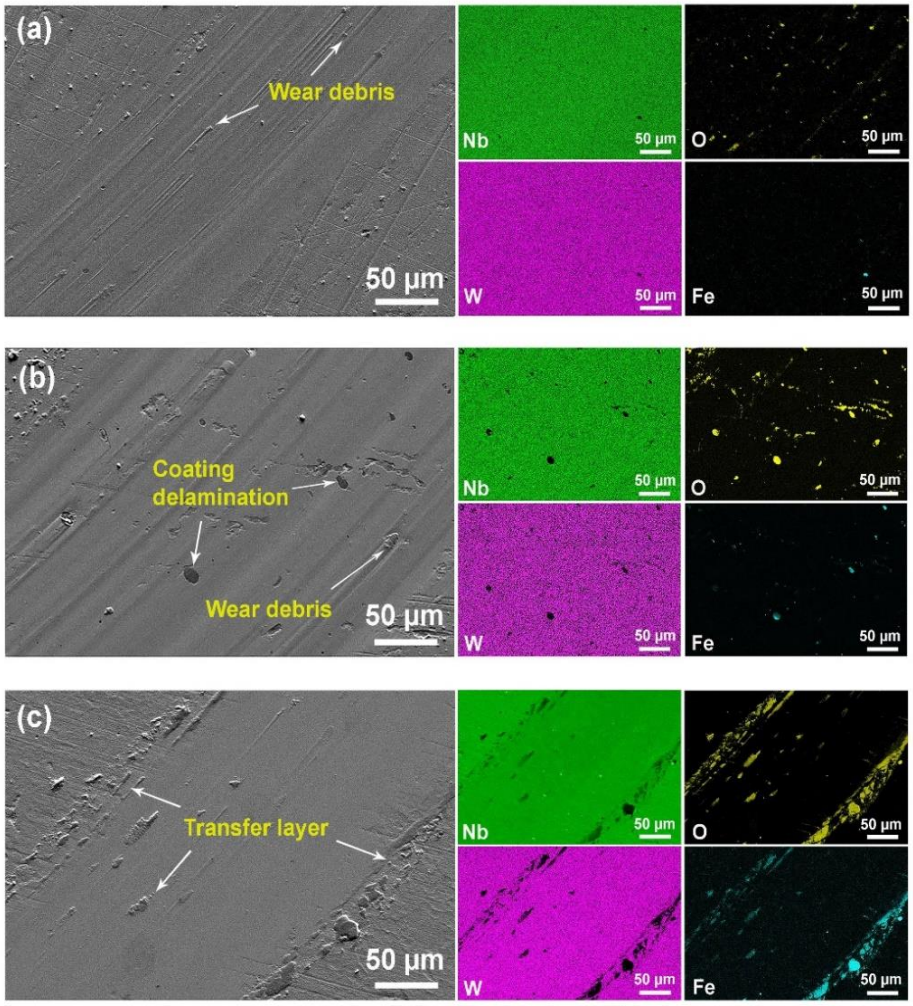

Fig. 12. *SEM images of the wear tracks of the WN/NbN multilayers and EDS elemental maps (smaller images on the right) after ball-on-disk tribotests as a function of substrate bias: –50 V (a), –100 V (b), and –200 V (c).*

The M-200 coating had different wear behavior from the other WN/NbN multilayers. It demonstrated a smooth with transfer layers on its surface, as seen in the SEM image (Fig. 12c) and 3D profile image (Fig. 13a). The calculated specific wear rate was about $3.2 \cdot 10^{-6}$ mm^3/Nm. Thus, its wear resistance fell between the other two coatings. After sliding against a stainless-steel ball, the coating surface was covered in transfer layers consisting of iron oxides, indicating adhesive wear as the main wear mechanism (Fig. 13d). It has been shown that Fe_3O_4 forming on the sliding surfaces acts as a protective oxide layer, reducing the wear rate. Moreover, along with a primary wear mechanism, the oxidative mode was also involved, improving the wear resistance.

It should be noted that multilayers were worn to different thicknesses. Comparing the GIXRD patterns (Fig. 9) and wear profiles (Fig. 13a), we could study the relationship between structural features and wear resistance of WN/NbN multilayers. Hence, we can conclude that a higher fraction of ε-NbN phase worsens the wear resistance of the studied coatings. Moreover, similar to mechanical properties, the preferred orientation of cubic grains along the (111) plane had a positive impact on wear behavior. Analysis of the wear behavior of the CA-PVD WN/NbN coatings demonstrated that the optimal thickness and bilayer period providing the best wear resistance were about 4.7 μm and 13 nm, respectively. Due to the high number of interfaces in the nanolayer architecture, small nanograins, negligible amount of hexagonal NbN crystallites, sufficient load-bearing capacity, and high

nanohardness, elastic strain to failure, and resistance to plastic deformation, the M-50 multilayer could effectively hinder crack propagation and withstand deformation and damage.

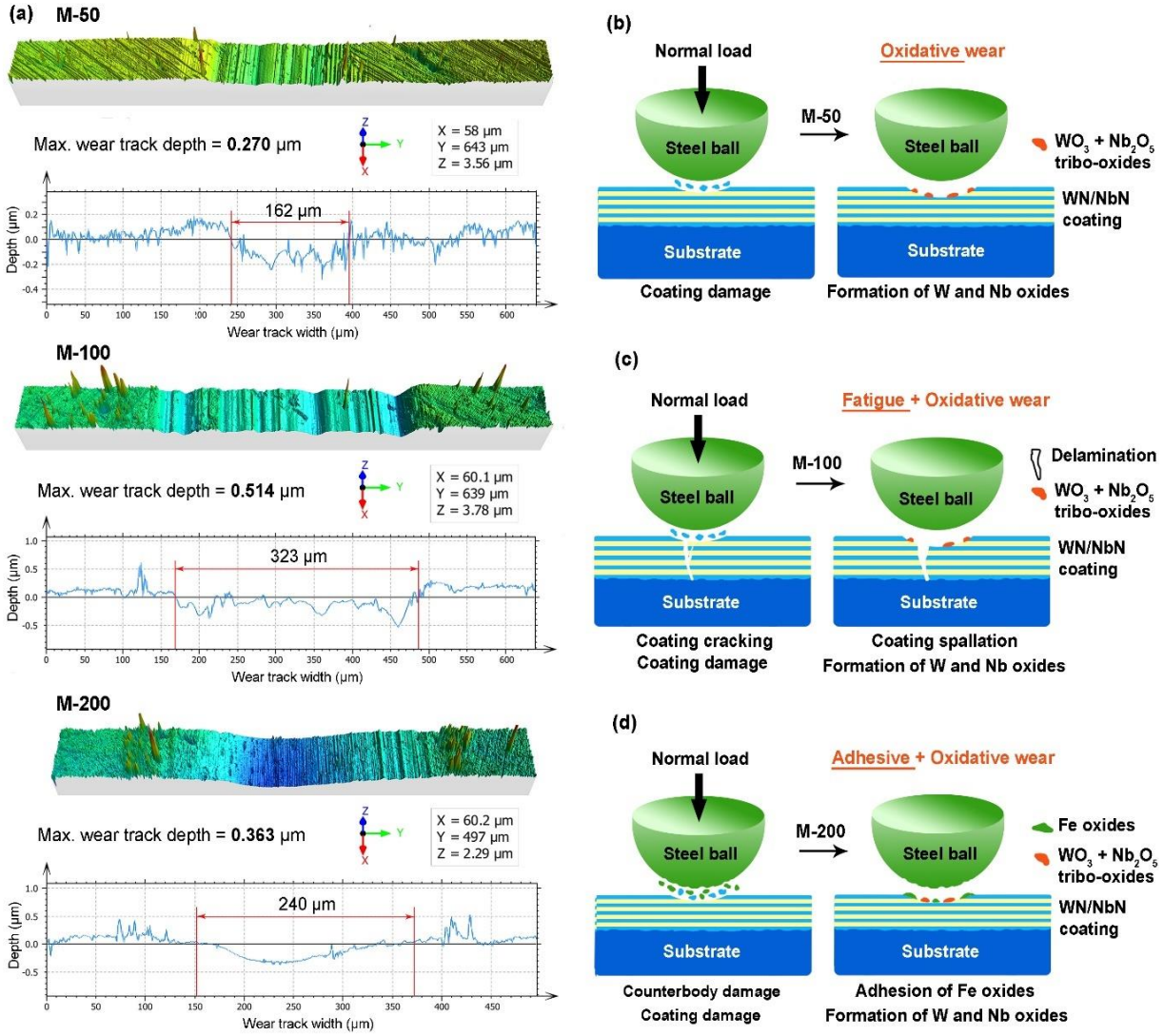

Fig. 13. *The 2D and 3D profiles of wear tracks of the CA-PVD WN/NbN nanolayer coatings deposited at different bias voltages (a). Wear mechanisms of the M-50 (b), M-100 (c), and M-200 (d) multilayers (the main wear mode is underlined).*

The formation of Nb_2O_5 and WO_3 oxides during the sliding process was confirmed by Raman spectroscopy. Spectra of the M-50 and M-200 multilayers obtained from wear debris, middle part and edges of wear tracks, and unworn coating surfaces were analyzed. All the Raman spectra accumulated on the flat area in the middle part of the wear tracks were very similar to the ones in the unworn regions, demonstrating NbN_x and W_2N phases. Along with W and Nb oxides, the M-200 coating exhibited the Fe_2O_3 and Fe_3O_4 on the surface of the wear scar, proving formation of transfer layers.

5. CONCLUSIONS

In this PhD thesis, the WN/MeN (Me = Cr, Zr, Mo, Nb) multilayer coatings deposited by CA-PVD have been comprehensively investigated. The effect of four different binary transition metal nitride layers on the microstructure, mechanical properties, friction performance, and wear behavior of WN-based multilayers can be summarized as follows:

1. Coatings could be roughly divided into two groups according to their microstructure: (i) all constituent layers had NaCl-type cubic structure (WN/Zr and WN/CrN), and (ii) WN layers consisted of the fcc W_2N phase, while other layers developed a combination of hexagonal and fcc NaCl-type cubic phases (δ-MoN, δ_3-MoN, and γ-Mo_2N in WN/MoN, as well as ε-NbN and δ-NbN in WN/NbN).
2. To substantiate the formation of the substoichiometric tungsten nitride layers in the deposited multilayers and to gain more insight into their properties, first-principles investigations of the stability, structure, and mechanical properties of the cubic random $W_{1-y}N_{1-x}$, $0 \leq x,y \leq 1$, phases were carried out. The results show that the tungsten nitride layers in the deposited coatings can be composed of disordered cubic WN_{1-x} structures with compositions close to $WN_{0.5}$. The $WN_{0.5}$ phase is elastically and dynamically stable and exhibits the properties inherent to ductile materials.
3. All coating systems exhibited a high hardness range from 33.3 ± 1.7 GPa to 37.3 ± 2.4 GPa. The maximum elastic strain to failure (H/E_r ratio) value of about 0.093 was observed for WN/NbN multilayer.
4. All coatings had similar friction coefficient values ranging from 0.47 to 0.55. The nanoscale WN/NbN coating showed the highest adhesion and had superior wear resistance. It exhibited the lowest specific wear rate of about $1.7 \cdot 10^{-6}$ mm^3/Nm. That could be related to a low roughness, high elastic strain to failure, more ductile behavior of NbN, the nanocomposite structure (ε-NbN and δ-NbN phases), and the formation of Nb_2O_5 and WO_3 tribofilms during sliding. The WN/ZrN coating showed the worst wear resistance.

Based on the first part of the research, the WN/NbN coating demonstrated its superiority over other studied WN-based multilayer systems. Thus, changes in structural features, mechanical properties, friction performance, and wear resistance of coatings deposited at various negative bias voltages in the 50-200 V range were comprehensively studied. The findings of an in-depth analysis can be summarized as follows:

1. Applying a negative bias voltage in the 50 – 200 V range resulted in variations in the total coating thickness (3.5 – 5.0 μm) and bilayer period (10 – 15 nm) of the deposited multilayers.
2. Coatings were characterized by a complex phase composition and texture evolution with increasing thickness due to different ion bombardment conditions. They were composed of the fcc β-W2N, δ-NbN, and hexagonal ε-NbN phases, confirmed by TEM analysis. The most drastic changes in the preferred orientation from (200) to (111) were observed in the coating deposited at the highest bias voltage and the lowest bilayer period (10 nm). Meanwhile, the M-100 multilayer with the highest Λ value of 15 nm demonstrated the least affected structure with a mixed (111) + (200)-texture and the highest amount of ε-NbN grains. Finally, in the case of the coating synthesized at the lowest energy of bombarding ions, most grains developed a (111)-orientation as the thickness increased. The fraction of the hexagonal phase significantly decreased to the point that it was undetectable by GIXRD in the 130 nm-thick top layer. Moreover, the residual stresses in deposited multilayers decreased from –6.93 ± 0.88 to –2.78 ± 0.56 GPa as the absolute value of the bias voltage increased. The texture features and increased mobility and diffusivity of adatoms contributed to the release of residual stresses.
3. STEM observations of the M-200 sample showed that interfaces between constituent WN and NbN layers were blurred, which could be caused by intermixing due to high-energetic conditions during deposition. Moreover, despite its complex structure, a multilayer attempted to achieve semi-coherence in the crystallites.
4. The nanohardness was the highest in the case of WN/NbN coating deposited at the highest bias voltage of –200 V (36.6 ± 3.5 GPa). However, high values of H/E_r and H^3/E_r^2 ratios were found to be more essential for wear-resistant coatings. Among all WN/NbN multilayers, the M-50 sample

demonstrated the maximum values of these parameters of 0.085 and 0.254, respectively. The formation of the (111) texture was found to have a positive effect on mechanical properties.

5. The analysis of the relationship between the microstructure and the increase in wear resistance of deposited WN/NbN coatings revealed the inversely proportional dependence on the portion of hard hexagonal grains. At the same time, the texture also had an effect. Coatings with (111)-oriented grains exhibited lower wear rate (M-50 and M-200 multilayers). Moreover, the H^3/E_r^2 ratio (resistance to plastic deformation) agreed well with wear resistance. As the absolute value of the negative bias voltage increased, the primary wear mechanism changed as follows: oxidative, fatigue, and adhesive modes. However, oxidative type of wear was inherent in all samples to varying degrees, which contributed to better wear resistance. As expected, the coating deposited at the lowest negative bias voltage exhibited the lowest specific wear rate of $1.9 \cdot 10^{-6}$ mm^3/Nm. This was attributed to the optimal thickness, bilayer period, high number of interfaces in the nanolayer architecture, small nanograins, the formation of lubricating "islands" of Nb_2O_5 and WO_3 during sliding, low volume fraction of the hexagonal NbN phase, (111) preferred orientation of the fcc grains, and high nanohardness, elastic strain to failure, and resistance to plastic deformation.

Therefore, based on the conducted analysis, it could be stated that elaborated CA-PVD WN-based nanolayer coatings hold significant promise as high-potential protective coatings suitable for tribological applications. These findings give space for further research since more simple materials allow us to predict peculiarities of the structure and properties of more complex nitrides.

REFERENCES

[1]. RASAKI, Sefiu Abolaji, Bingxue ZHANG, Kousika ANBALGAM, Tiju THOMAS and Minghui YANG. Synthesis and application of nano-structured metal nitrides and carbides: A review. Progress in Solid State Chemistry [online]. 2018, vol. 50, pp. 1–15. ISSN 00796786. Available at: doi:10.1016/j.progsolidstchem.2018.05.001

[2]. POLCAR, T. and A. CAVALEIRO. Structure, mechanical properties and tribology of W–N and W–O coatings. International Journal of Refractory Metals and Hard Materials [online]. 2010, vol. 28, no. 1, pp. 15–22. ISSN 02634368. Available at: doi:10.1016/j.ijrmhm.2009.07.013

[3]. MUSIL, Jindřich, Martin JAROŠ, Radomír ČERSTVÝ and Stanislav HAVIAR. Evolution of microstructure and macrostress in sputtered hard Ti(Al,V)N films with increasing energy delivered during their growth by bombarding ions. Journal of Vacuum Science & Technology A: Vacuum, Surfaces, and Films [online]. 2017, vol. 35, no. 2, p. 020601. ISSN 0734-2101. Available at: doi:10.1116/1.4967935

[4]. POGREBNJAK, Alexander, Kateryna SMYRNOVA and Oleksandr BONDAR. Nanocomposite Multilayer Binary Nitride Coatings Based on Transition and Refractory Metals: Structure and Properties. Coatings [online]. 2019, vol. 9, no. 3, p. 155. ISSN 2079-6412. Available at: doi:10.3390/coatings9030155

[5]. GONZÁLEZ-CARMONA, J. M., J. D. TRIVIÑO, Á GÓMEZ-OVALLE, C. ORTEGA, J. M. ALVARADO-OROZCO, H. SÁNCHEZ-STHEPA and A. AVILA. Wear mechanisms identification using Kelvin probe force microscopy in TiN, ZrN and TiN/ZrN hard ceramic multilayers coatings. Ceramics International [online]. 2020, vol. 46, no. 15, pp. 24592–24604. ISSN 02728842. Available at: doi:10.1016/j.ceramint.2020.06.248

[6]. DU, Jian W., Li CHEN, Jie CHEN and Yong DU. Mechanical properties, thermal stability and oxidation resistance of TiN/CrN multilayer coatings. Vacuum [online]. 2020, vol. 179, p. 109468. ISSN 0042207X. Available at: doi:10.1016/j.vacuum.2020.109468

[7]. LI, D. J., F. LIU, M. X. WANG, J. J. ZHANG and Q. X. LIU. Structural and mechanical properties of multilayered gradient CrN/ZrN coatings. Thin Solid Films [online]. 2006, vols. 506–507, pp. 202–206. ISSN 00406090. Available at: doi:10.1016/j.tsf.2005.08.031

[8]. ZHANG, Guojun, Tao WANG and Hailin CHEN. Microstructure, mechanical and tribological properties of TiN/Mo2N nano-multilayer films deposited by magnetron sputtering. Surface and Coatings Technology [online]. 2015, vol. 261, pp. 156–160. ISSN 02578972. Available at: doi:10.1016/j.surfcoat.2014.11.041

[9]. KUMAR, D. Dinesh, N. KUMAR, S. KALAISELVAM, S. DASH and R. JAYAVEL. Wear resistant super-hard multilayer transition metal-nitride coatings. Surfaces and Interfaces [online]. 2017, vol. 7, pp. 74–82. ISSN 24680230. Available at: doi:10.1016/j.surfin.2017.03.001

[10]. STUEBER, M., H. HOLLECK, H. LEISTE, K. SEEMANN, S. ULRICH and C. ZIEBERT. Concepts for the design of advanced nanoscale PVD multilayer protective thin films. Journal of Alloys and Compounds [online]. 2009, vol. 483, nos. 1–2, pp. 321–333. ISSN 09258388. Available at: doi:10.1016/j.jallcom.2008.08.133

[11]. POGREBNJAK, Alexander D., Volodymyr I. IVASHCHENKO, Petro L. SKRYNSKYY, Oleksandr V. BONDAR, Piotr KONARSKI, Karol ZAŁĘSKI, Stefan JURGA and Emerson COY. Experimental and theoretical studies of the physicochemical and mechanical properties of multi-layered TiN/SiC films: Temperature effects on the nanocomposite structure. Composites Part B: Engineering [online]. 2018, vol. 142, pp. 85–94. ISSN 13598368. Available at: doi:10.1016/j.compositesb.2018.01.004
[12]. CUI, Zi-Jing, Dao-Lin CAI, Yang LI, Cheng-Xing LI and Zhi-Tang SONG. WN coating of TiN electrode to improve the reliability of phase change memory. Materials Science in Semiconductor Processing [online]. 2022, vol. 138, p. 106273. Available at: doi:10.1016/j.mssp.2021.106273
[13]. WANG, Changchun, Qiang TAO, Yan LI, Shuailing MA, Shushan DONG, Tian CUI, Xin WANG and Pinwen ZHU. Excellent mechanical properties of metastable c-WN fabricated at high pressure and high temperature. International Journal of Refractory Metals and Hard Materials [online]. 2017, vol. 66, pp. 63–67. ISSN 02634368. Available at: doi:10.1016/j.ijrmhm.2017.02.004
[14]. MOHARANA, P. L., Sharmistha ANWAR, Aminul ISLAM and Shahid ANWAR. Structural and mechanical study of thermally annealed tungsten nitride thin films. Perspectives in Science [online]. 2016, vol. 8, pp. 636–638. Available at: doi:10.1016/j.pisc.2016.06.042
[15]. KURBATOV, D., A. OPANASYUK and H. KHLYAP. Substrate-temperature effect on the microstructural and optical properties of ZnS thin films obtained by close-spaced vacuum sublimation. physica status solidi (a) [online]. 2009, vol. 206, no. 7, pp. 1549–1557. ISSN 1862-6300. Available at: doi:10.1002/pssa.200824472
[16]. ZUKOWSKI, Pawel, Tomasz N. KOLTUNOWICZ, Vitalii BONDARIEV, Alexander K. FEDOTOV and Julia A. FEDOTOVA. Determining the percolation threshold for (FeCoZr)x(CaF2)(100−x) nanocomposites produced by pure argon ion-beam sputtering. Journal of Alloys and Compounds [online]. 2016, vol. 683, pp. 62–66. Available at: doi:10.1016/j.jallcom.2016.05.070
[17]. HASHMI, S. Comprehensive Materials Processing. 1st ed. B.m.: Elsevier. ISBN 978-0-08-096532-1.
[18]. HOLLECK, H. Material selection for hard coatings. Journal of Vacuum Science & Technology A [online]. 1986, vol. 4, no. 6, pp. 2661–2669. Available at: doi:10.1116/1.573700
[19]. GAFFNEY, Jeffrey S. and Nancy A. MARLEY. Chapter 3 - Chemical Bonding—The Formation of Materials. In: Jeffrey S. GAFFNEY and Nancy A. MARLEY, eds. General Chemistry for Engineers [online]. B.m.: Elsevier, p. 75–116. Available at: doi:10.1016/B978-0-12-810425-5.00003-5
[20]. WEBER, Matthieu, Igor IATSUNSKYI, Emerson COY, Philippe MIELE, David CORNU and Mikhael BECHELANY. Novel and Facile Route for the Synthesis of Tunable Boron Nitride Nanotubes Combining Atomic Layer Deposition and Annealing Processes for Water Purification. Advanced Materials Interfaces [online]. 2018, vol. 5, no. 16, p. 1800056. Available at: doi:10.1002/admi.201800056
[21]. BOING, Denis, Adilson José DE OLIVEIRA and Rolf Bertrand SCHROETER. Limiting conditions for application of PVD (TiAlN) and CVD (TiCN/Al2O3/TiN) coated cemented carbide grades in the turning of hardened steels. Wear [online]. 2018, vols. 416–417, pp. 54–61. Available at: doi:10.1016/j.wear.2018.10.007
[22]. VERESCHAKA, Alexey, Vladimir TABAKOV, Sergey GRIGORIEV, Nikolay SITNIKOV, Gaik OGANYAN, Nikolay ANDREEV and Filipp MILOVICH. Investigation of wear dynamics for cutting tools with multilayer composite nanostructured coatings in turning constructional steel. Wear [online]. 2019, vols. 420–421, pp. 17–37. Available at: doi:10.1016/j.wear.2018.12.033
[23]. JAVDOŠŇÁK, D., J. MUSIL, Z. SOUKUP, S. HAVIAR, R. ČERSTVÝ and J. HOUSKA. Tribological properties and oxidation resistance of tungsten and tungsten nitride films at temperatures up to 500 °C. Tribology International [online]. 2019, vol. 132, pp. 211–220. ISSN 0301679X. Available at: doi:10.1016/j.triboint.2018.12.019
[24]. GOLIZADEH, Mehran, André ANDERS, Francisca Mendez MARTIN, Szilard KOLOZSVÁRI and Robert FRANZ. Insights into surface modification and erosion of multi-element arc cathodes using a novel multilayer cathode design. Journal of Applied Physics [online]. 2020, vol. 127, no. 11, p. 113301. ISSN 0021-8979. Available at: doi:10.1063/1.5141406
[25]. RAFAJA, D., C. WÜSTEFELD, C. BAEHTZ, V. KLEMM, M. DOPITA, M. MOTYLENKO, C. MICHOTTE and M. KATHREIN. Effect of Internal Interfaces on Hardness and Thermal Stability of Nanocrystalline Ti0.5Al0.5N Coatings. Metallurgical and Materials Transactions A [online]. 2011, vol. 42, no. 3, pp. 559–569. ISSN 1073-5623, 1543-1940. Available at: doi:10.1007/s11661-010-0204-8
[26]. ABDOOS, Majid, Bipasha BOSE, Sushant RAWAL, Abul Fazal M. ARIF and Stephen C. VELDHUIS. The influence of residual stress on the properties and performance of thick TiAlN multilayer coating during dry turning of compacted graphite iron. Wear [online]. 2020, vols. 454–455, p. 203342. ISSN 00431648. Available at: doi:10.1016/j.wear.2020.203342

ABSTRACT

The dissertation thesis aims to comprehensively study the effect of a second MeN (Me = Zr, Cr, Mo, Nb) layer in WN-based nanocomposite multilayer coatings on their microstructure, phase composition, mechanical properties, and tribological performance. Moreover, an in-depth analysis of the WN/NbN coatings the structure–tribomechanical properties relationship and evolution of texture with increasing thickness depending on the ion bombardment conditions was conducted. The cathodic-arc evaporation (CA-PVD) has been used to deposit proposed coating systems on polished stainless-steel substrates for the first time. Additionally, first-principles calculations were performed to gain more insight into the structural and mechanical properties of the cubic tungsten nitride. The obtained results establish a robust foundation for elucidating the correlation between structure and properties in binary multilayer coatings based on proposed transition metals. Furthermore, the implementation of designed WN/NbN multilayers with superior properties presents an opportunity to eliminate the shortcomings inherent existing protective coatings utilized under extreme conditions.

This work consists of 5 chapters. The first chapter is devoted to a review of multilayer nitride coatings. The second chapter describes the main goals of the Ph.D. thesis. The third chapter describes the methodology used to investigate the structure and properties of the deposited coating. The fourth chapter includes all the results of a comprehensive study of WN-based multilayer nanostructured coatings. Finally, the fifth chapter provides conclusions with the purpose of future research.

Keywords: multilayer coatings, nitrides, hard coatings, PVD, cathodic-arc evaporation, nanohardness, microstructure, adhesion, wear.

SÚHRN

Cieľom dizertačnej práce je detailné štúdium vplyvu sekundárnej vrstvy MeN (Me = Zr, Cr, Mo a Nb) nanokompozitných multivrstvových povlakov na báze nitridu volfrámu (WN) na ich mikroštruktúru, fázové a chemické zloženie, mechanické a tribologické vlastnosti. Navyše, v práci bol detailne sledovaný vplyv štruktúry na tribologické vlastnosti, ako aj vývoj textúry v uvedených multivrstvách v závislosti od ich hrúbky ovplyvnenej podmienkami iónového bombardovania. Metóda katódového oblúkového naparovania (CA-PVD) bola prvýkrát použitá s cieľom vyhotovenia týchto typov povlakov. Ako substrát bola využitá koróziivzdorná oceľ. Za účelom analýzy štruktúrnych a mechanických vlastností povlaku kubického nitridu volfrámu (WN), boli aplikované výpočty z prvých princípov, tzv. "Ab-initio." Dosiahnuté výsledky pomáhajú stanoviť a objasniť vzťahy medzi štruktúrou a vybranými vlastnosťami binárnych multivrstvových povlakov na báze nitridov prechodových kovov. Navyše, aplikácia multivrstiev so zlepšenými vlastnosťami predstavuje príležitosť na odstránenie nedostatkov v súčasnosti používaných povlakov pracujúcich v extrémnych podmienkach.

Dizertačná práca pozostáva z 5 kapitol. Prvá kapitola poskytuje teoretický prehľad o multivrstvách na báze nitridov prechodových prvkov. Druhá kapitola popisuje hlavné ciele doktorandského štúdia. V tretej kapitole sú zhrnuté metódy využité v rámci skúmania štruktúry a vlastností multivrstiev. Štvrtá kapitola komplexne pojednáva o výsledkoch dosiahnutých v priebehu riešenia experimentálnej časti dizertačnej práce. Poslednou kapitolou je záver, s návrhmi budúceho smerovania výskumných aktivít.

Kľúčové slová: viacvrstvové povlaky, nitridy, tvrdé povlaky, PVD, katódové oblúkové naparovanie, nanotvrdosť, mikroštruktúra, adhézia, opotrebenie.

LIST OF PUBLICATIONS

1. **SMYRNOVA, K.**, SAHUL, M., HARŠÁNI, M., POGREBNJAK, A., ČAPLOVIČ, Ľ., BERESNEV, V., ČAPLOVIČOVÁ, M., KUSÝ, M. Effect of Bias Voltage on the Structural Properties of WN/NbN nanolayer Coatings Deposited by Cathodic-arc Evaporation. *Journal of Physics: Conference Series*, in press.

2. **SMYRNOVA, K.**, SAHUL, M., HARŠÁNI, M., BERESNEV, V., TRUCHLÝ, M., STOLBOVOY, V., ČAPLOVIČ, Ľ., ČAPLOVIČOVÁ, M., KUSÝ, M., KOZAK, A., FLOCK, D., POGREBNJAK, A. Composite materials with nanoscale multilayer architecture based on cathodic-arc evaporated WN/NbN coatings. Submitted to *Advanced Materials Interfaces*.

3. **SMYRNOVA, K.**, SAHUL, M., HARŠÁNI, M., POGREBNJAK, A., IVASHCHENKO, V., BERESNEV, V., STOLBOVOY, V., ČAPLOVIČ, Ľ., ČAPLOVIČOVÁ, M., VANČO, Ľ., KUSÝ, M., KASSYMBAEV, A. SATRAPINSKYY, L., FLOCK, D.. Microstructure, Mechanical and Tribological Properties of Advanced Layered WN/MeN (Me = Zr, Cr, Mo, Nb) Nanocomposite Coatings. *Nanomaterials*, 2022, 12 (3), 395 (1-23). ISSN 2079-4991. (11 citations).

4. SAHUL, M., BOČÁKOVÁ, B., **SMYRNOVA, K.**, HARŠÁNI, M., SAHUL, M., TRUCHLÝ, M., KUSÝ, M., POGREBNJAK, A., ČAPLOVIČ, Ľ., VOPÁT, T. The influence of multilayer architecture on the structure and mechanical properties of WN_x/TiSiN coatings in comparison with WN_x and TiSiN single layers. *Journal of Physics: Conference Series*. 2022, 2413, Development of Materials Science in Research and Education (DMSRE31 2022), 012013 (1-8). (0 citations).

5. POSTOLNYI, B., BURANICH, V., **SMYRNOVA, K.**, ARAÚJO, J.P., REBOUTA, L., POGREBNJAK, A., ROGOZ, V. Multilayer and high-entropy alloy-based protective coatings for solving the issue of critical raw materials in the aerospace industry. *IOP Conference Series: Materials Science and Engineering*, 2020, 1024, 10th EASN International Conference on Innovation in Aviation and Space to the Satisfaction of the European Citizens, 012009 (1-8). (7 citations).

6. POGREBNJAK, A., **SMYRNOVA, K.**, BONDAR, O. Nanocomposite multilayer binary nitride coatings based on transition and refractory metals: Structure and properties. *Coatings*. 2019, 9 (3), 155 (1-27). ISSN 2079-6412. (44 citations).

7. **SMYRNOVA, K.**, SAHUL, M., HARŠÁNI, M., POGREBNJAK, A., ČAPLOVIČ, Ľ., BERESNEV, V., ČAPLOVIČOVÁ, M., KUSÝ, M. Tribological performance of nanolaminate coatings based on tungsten and niobium nitrides. In *Development of Materials Science in Research and Education (DMSRE 2023)*, 4 – 8 September 2023, Pavlov, Czechia, 63. ISBN 978-80-907237-4-0.

8. **SMYRNOVA, K.**, SAHUL, M., HARŠÁNI, M., POGREBNJAK, A., ČAPLOVIČ, Ľ., BERESNEV, V., ČAPLOVIČOVÁ, M., KUSÝ, M. Multilayer Nanoscale WN/NbN Coatings with Superior Mechanical Properties and Wear Performance. In *13th International Conference "Nanomaterials: Applications & Properties" (IEEE NAP - 2023)*, 10-15 September 2023. Braatislava, Slovakia, 03mtfc-1.

9. SAHUL, M., **SMYRNOVA, K.**, HARŠÁNI, M., SAHUL, M., BOČÁKOVÁ, B., VASHCHUK, A., POGREBNJAK, A., ČAPLOVIČOVÁ, M., ČAPLOVIČ, Ľ. Synthesis & Characterization of WN/TiSiN Nanocomposite Multilayer Coatings. In *12th International Conference "Nanomaterials: Applications & Properties" (IEEE NAP - 2022)*, 11-16 September 2022. Kraków, Poland, 154.

10. **SMYRNOVA, K.**, SAHUL, M., HARŠÁNI, M., POGREBNJAK, A., ČAPLOVIČ, Ľ., SAHUL, M. WN/TiSiN Nanostructured Coating for Severe Tribological Applications. In *12th International Conference "Nanomaterials: Applications & Properties" (IEEE NAP - 2022)*, 11-16 September 2022, Kraków, Poland, 159.

11. **SMYRNOVA, K.**, SAHUL, M., HARŠÁNI, M., POGREBNJAK, A., BERESNEV, V., ČAPLOVIČ, Ľ. The Effect of Bias Voltage on Structure and Mechanical Properties of WN/NbN Multilayers. In *11th International Conference "Nanomaterials: Applications & Properties" (NAP-2021*), 5-11 September 2021, Odesa, Ukraine, 5. ISBN 978-1-6654-3907-7.

12. POSTOLNYI, B., BURANICH, V., **SMYRNOVA, K.**, ARAÚJO, J.P., POGREBNJAK, A., ROGOZ, V. Multilayer and High-Entropy Alloy-Based Coatings for Solving the Critical Raw Materials Problem. In *10th International*

Conference "Nanomaterials: Applications & Properties" (NAP-2020), 9-13 November 2020, Sumy, Ukraine, 03TFC07-1.

13. **SMYRNOVA, K.**, SAHUL, M., POGREBNJAK, A., BERESNEV, V., STOLBOVOY, V., ČAPLOVIČ, Ľ., KUSÝ, M., HARŠÁNI, M. Microstructure and Tribomechanical Properties of WN-based Binary Multilayer Protective Coatings. In *10th International Conference "Nanomaterials: Applications & Properties" (NAP-2020*), 9-13 November 2020, Sumy, Ukraine, 03TFC01-1.

14. POSTOLNYI, B., BURANICH, V., Klaver, P., **SMYRNOVA, K.**, REBOUTA, L., ARAÚJO, J.P., POGREBNJAK, A., ROGOZ, V. High-entropy Alloys and Coatings for Mitigation of Critical Raw Materials Problem: Prediction of their Stability and Properties. In *3rd International Conference on Emerging Technologies in Materials Engineering*, 29-30 October 2020, Bucharest, Romania, 99. ISSN 2602-0424.

Other publications

15. DIEDKOVA, K., POGREBNJAK, A., KYRYLENKO, S., **SMYRNOVA, K.**, BURANICH, V.V., HORODEK, P., ZUKOWSKI, P., KOLTUNOWICZ, T.N., GALASZKIEWICZ, P., MAKASHINA, K., BONDARIEV, V., SAHUL, M., ČAPLOVIČOVÁ, M., HUSAK, Y., SIMKA, W., KORNIIENKO, V., STOLARCZYK, A., BLACHA-GRZECHNIK, A., BALITSKYI, V., ZAHORODNA, V., BAGINSKIY, I., RIEKSTINA, U., GOGOTSI, O., GOGOTSI, Y., POGORIELOV, M. Polycaprolactone–MXene Nanofibrous Scaffolds for Tissue Engineering. *ACS Applied Materials & Interfaces*, 2023. 15 (11), 14033-14047. ISSN 1944-8244. (10 citations).

16. POGORIELOV, M., **SMYRNOVA, K.**, KYRYLENKO, S., GOGOTSI, O., ZAHORODNA, V., POGREBNJAK, A. Mxenes—a new class of two-dimensional materials: Structure, properties and potential applications. *Nanomaterials*, 2021, 11 (12), 1-57. ISSN 2079-4991. (34 citations).

17. SAHUL, M., **SMYRNOVA, K.**, HARŠÁNI, M., ČAPLOVIČ, Ľ., POGREBNJAK, A., SAHUL, M., KUSÝ, M., BABINCOVÁ, P., VOPÁT, T. Effect of lanthanum addition on the structure evolution and mechanical properties of the nanocomposite Ti-Si-N coatings. *Materials Letters*, 2020, 276, 1-4. ISSN 0167-577X. (9 citations).

18. GRITSENKO, B.P., RECHENKO, D.S., ROGACHEV, E.A., **SMYRNOVA, K.V**., BAGDASARYAN, A.A., SERGEEV, V.P., POPOV, A.Yu., NOGAIBEKOVA, G.Zh., FEDORISCHEVA, M.V., POGREBNJAK, A.D. Enhancement of the Wear Resistance of Tungsten Cobalt Carbide Plates Using Ion Implantation and Al–Si–N Coatings. In *Springer Proceedings in Physics*. *Microstructure and Properties of Micro-and Nanoscale Materials, Films, and Coatings (NAP 2019) Selected Articles from the International Conference on Nanomaterials: Applications and Properties*,*(NAP 2019)*, 2020, Springer Singapore, 279-286. ISBN 978-981151741-9. (1 citation).

19. **SMYRNOVA, K.V.**, Pogrebnjak, A.D., Kassenova L.G. Structural features and properties of biocompatible Ti-based alloys with β-stabilizing elements. In *Lecture Notes in Mechanical Engineering. Advances in Thin Films, Nanostructured Materials, and Coatings: Selected Papers from the 2018 International Conference on "Nanomaterials: Applications & Properties"*, 2019, Springer Singapore, 319-330. ISSN 21954356. (4 citations).

20. **SMYRNOVA, K**, POGREBNJAK, A., LOBODA, V., SHELEST, I., STOLBOVOY, V. Microstructural Analysis of the Multilayer (TiAlCrY/Zr)N Protective Coatings. In *11th International Conference "New electrical and Electronic Technologies and their Industrial Implementation" (NEET-2019)*, 25-28 June 2019, Zakopane, Poland, 72.

21. **SMYRNOVA, K.**, POGREBNJAK, A., OPIELAK, M., BUDZYŃSKI, P., BAGDASARYAN, A., LOBODA, V., SHELEST, I., STOLBOVOY, V. The Effect of the Layer Thickness on Elemental Composition and Structure of the Multilayer (TiAlCrY/Zr)N Coatings. In 9th International Conference "Nanomaterials: Applications & Properties" (NAP-2019),15-20 September 2019, Odessa, Ukraine, IDNUM-1.

22. **SMYRNOVA, K.**, POGREBNJAK, A., BERESNEV, V., LITOVCHENKO, S., BORBA-POGREBNJAK, S., MANOKHIN, A., KLIMENKO, S., ZHOLLYBEKOV, B., KUPCHISHIN, A., Kravchenko, Y., BONDAR, O. Microstructure and Physical–Mechanical Properties of (TiAlSiY)N Nanostructured Coatings Under Different Energy Conditions. *Metals and Materials International*, 2018, 24 (5), 1024–1035. ISSN 1598-9623. (26 citations).

23. POGREBNJAK, A., BERESNEV, V., **SMYRNOVA, K.**, Kravchenko, Y., ŻUKOWSKI, P., BONDARENKO, G. The influence of nitrogen pressure on the fabrication of the two-phase superhard nanocomposite (TiZrNbAlYCr)N coatings. *Materials Letters*, 2018, 211, 316-318. ISSN 0167-577X. (71 citations). ADC

24. BONDARIEV, V., POGREBNJAK, A., BERESNEV, V.M., LITOVCHENKO, S.V., BORBA-POGREBNJAK, S.O., **SMYRNOVA, K.V**. Influence of bias potential on the tribological behavior and physical-mechanical properties of TiAlSiY-based nanostructured coatings. In *Advanced Topics in Optoelectronics, Microelectronics, and Nanotechnologies IX*. - SPIE, 2018, 10977, 355-364. ISBN 978-151062613-3. (0 citations).

25. KRAVCHENKO, Y., BORYSIUK, V., POGREBNJAK, A., KYLYSHKANOV, M., IATSUNSKYI, I., **SMYRNOVA, K**. Characteristics of Arc-PVD TiAlSiY and (TiAlSiY)N coatings. In Proceedings of the *2017 IEEE 7th International Conference Nanomaterials: Application & Properties*, *NAP-2017*, 2017-January, 01FNC02 (1-4). ISBN 978-153862810-2. (2 citations).

26. **SMYRNOVA, K.V.**, BONDAR, O.V., BORBA-POGREBNJAK, S.O., KRAVCHENKO, Y.O., BERESNEV, V.M., ZHOLLYBEKOV, B., BAIMOLDANOVA, L. Process of Formation of Spheroidal Gold Particles and of Nanophases in AlN-TiB_2-$TiSi_2$ Coatings after Annealing with Subsequent Implantation. In Proceedings of the *2017 IEEE 7th International Conference Nanomaterials: Application & Properties, NAP-2017*, 2017-January, 01FNC13 (1-4). ISBN 978-153862810-2. (0 citations).

27. DEMIANENKO, A., SMYRNOVA, K., ZHOLLYBEKOV, B., KUPCHISHIN, A., TAKEDA, Y., AMEKURA, H., KOMSTA, H., OPIELAK, M., KIERCZYNSKI, K. Process of formation of spheroidal gold particles and of nanophases in AlN-TiB_2-$TiSi_2$ coatings after annealing with subsequent implantation. *High Temperature Material Processes*, 2015, 19 (2), 189-200. ISSN 1093-3611. (11 citations).

28. **SMYRNOVA, K.V.**, DEMIANENKO, A.A., RADKO, A.S., PSHYK, A.V., KUZOVLEV, O.V., AMEKURA, H., OYOSHI K., TAKEDA, Y. The Influence of the Ion Implantation of AU- to the Microstructure of the Amorphous-Nanocrystaline AlN-TiB_2-$TiSi_2$. *Journal of Nano- and Electronic Physics*, 2015, 7 (1), 01040 (1-5). ISSN 20776772. (8 citations).

29. POGREBNJAK, A.D., BORISYUK, V.N., BAGDASARYAN, A.A., MAKSAKOVA, O.V., **SMIRNOVA, E.V.** The Multifractal Investigation of Surface Microgeometry of (Ti-Hf-Zr-V-Nb)N Nitride Coatings. *Journal of Nano-& Electronic Physics*, 2014, 6 (4), 04018 (1-4). ISSN 20776772. (14 citations).

30. BAGDASARYAN, A.A, **SMIRNOVA, E.**, KONARSKI, P., MIŚNIK, M., ZAWADA, A. The Analysis of Elemental Composition and Depth Profiles of Nitride Nanostructured Coating based on the TiHfVNbZr High-entropy Alloy. *Journal of Nano-& Electronic Physics*, 2014, 6 (2), 02028 (1-5). ISSN 20776772. (10 citations).